GeoScienceWorld
Lithosphere
Volume 2020, Article ID 8844754, 33 pages
https://doi.org/10.2113/2020/8844754

Lithosphere

Research Article

Eustatic, Climatic, and Oceanographic Influences on Geomorphology and Architecture of Isolated Carbonate Platforms: Miocene, Northwest Shelf, Australia

Eugene C. Rankey

Kansas Interdisciplinary Carbonates Consortium, Department of Geology, University of Kansas, Lawrence, KS 66045, USA

Correspondence should be addressed to Eugene C. Rankey; grankey@ku.edu

Received 11 July 2020; Accepted 12 November 2020; Published 17 December 2020

Academic Editor: Jean Borgomano

The Miocene represents an interval of marked global change, and this evolution is reflected in carbonate platforms from this epoch. Seismic stratigraphic characterization of high-resolution (*ca* 60 Hz) 3D seismic data from the Browse Basin, offshore Australia, reveals a middle to upper Miocene three-part seismic stratigraphic subdivision. Each unit consists of several seismic sequence sets and their component sequences. Seismic stratal geometries and seismic facies define a prograding shelf (Langhian and older), a barrier-reef complex with scattered platforms (upper Langhian–early Tortonian), and aggrading and prograding isolated platforms (early Tortonian–Messinian). The data permit description and interpretation of high-fidelity stratigraphic details of the initiation, expansion, termination, and geomorphology of over 100 platforms in this interval. The results reveal that the isolated platforms initiated following the Middle Miocene Climatic Optimum. The succession includes major seismic stratigraphic boundaries and overall patterns of platform growth and demise that correspond roughly with periods of pronounced eustatic change associated with initiation of eastern Antarctic ice sheets. Although invoking a eustatic control for coarse trends may be tempting, mismatch between the numbers and ages of sequences, as well as the variable stacking patterns among contemporaneous platforms regionally, precludes such an interpretation; conversely, some globally recognized eustatic changes do not have a pronounced manifestation in this area. Thus, it appears that the eustatic signal combined with dynamic physical regional processes such as waves, currents, and variable subsidence creates the complex architecture and geomorphology of platforms. These results illustrate how global changes can interact with local controls to create diverse patterns of birth, growth, and demise of carbonate platforms and drive local stratal heterogeneity.

1. Introduction

Isolated platforms represent large-scale edifices constructed largely by the activity of organisms. As such, they provide records of any process that influences the flora and fauna or controls the accumulation of sediment derived from their skeletons [1–6].

As sensitive recorders, isolated carbonate platforms offer the potential to provide insights into the dynamics of pronounced changes in the Earth system. For example, during the Miocene (Figure 1(a)) [7–12], a gradual global warming from the late Oligocene culminated in the Middle Miocene Climate Optimum, a marked warm period [12], with some of the highest eustatic levels of the Cenozoic. Shortly thereafter, global climate started to cool [12], and by late Miocene, the Antarctic Ice Sheet started to expand markedly, followed by growth of the northern hemisphere ice sheets and the West Antarctic Ice Sheet in the latest Miocene to Pliocene. This buildup of land-based ice sheets led to generally falling sea level [13] and higher amplitudes of change, in the latest Miocene to present. As these changes were occurring, tectonic activity in the Tethys, Caribbean-Pacific, and Southeast Asia limited equatorial current exchange between ocean basins and modified global oceanic circulation patterns [14–16]. Coupled with other tectonic influences such as uplift of the Tibetan Plateau, opening of the South China Sea, and northward drift of the Australian plate, these changes drove the initiation and intensity of atmospheric systems such as

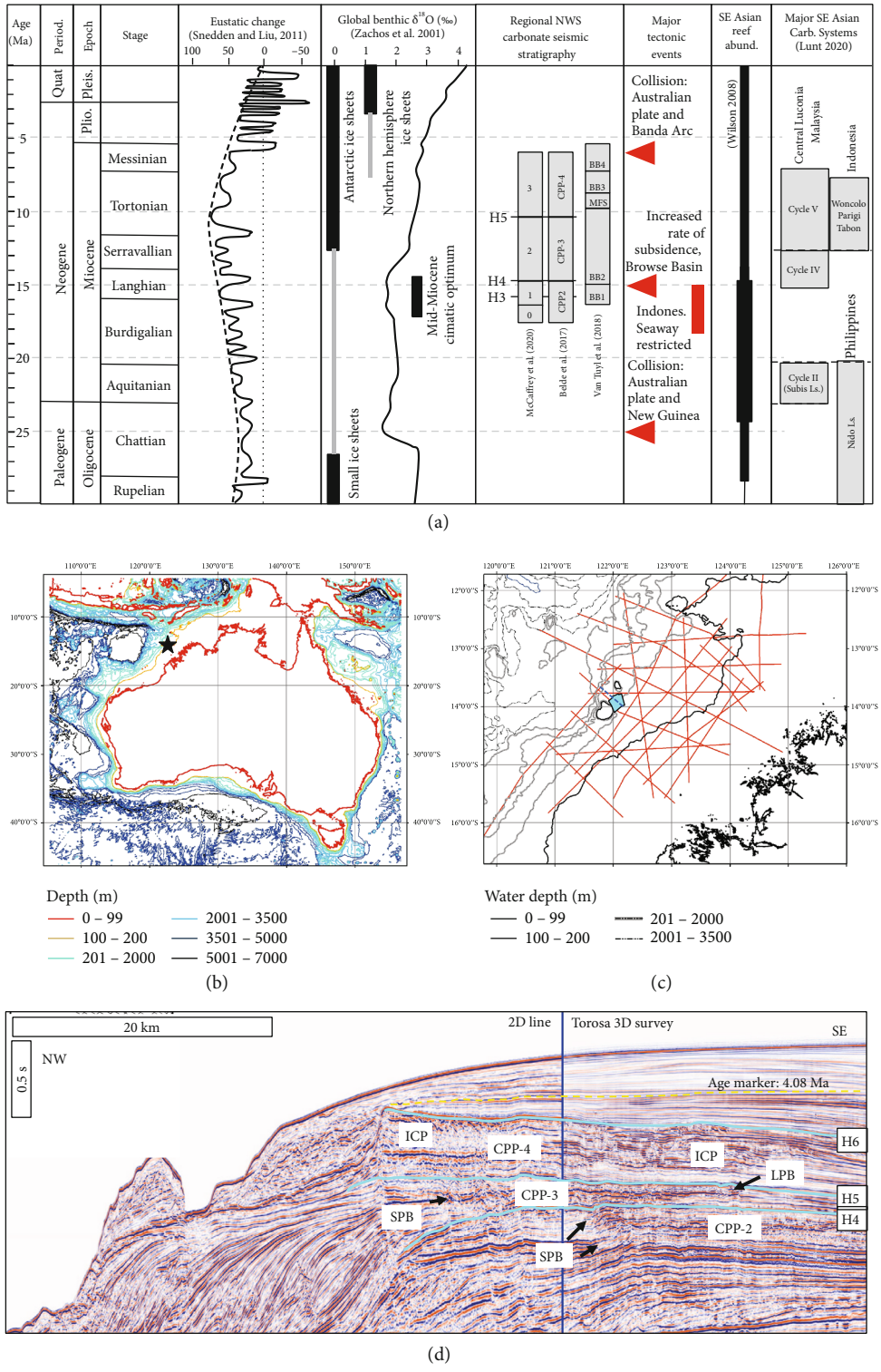

FIGURE 1: General global and geographic setting of the study. (a) Chart summarizing relevant Cenozoic global trends, including (i) eustasy (Snedden and Liu [13, 78]); (ii) paleoclimate, including global benthic $\delta^{18}O$ [12], (iii) stratigraphy, including regional interpretations of stratigraphy on the Northwest Shelf [25, 28, 29], and (iv) major regional tectonic events that impacted the Northwest Shelf; (v) abundance of Southeast Asian reefs [37]; and (vi) selected Southeast Asian stratigraphic and reservoir units of these ages (Lunt 2020). (b) Location map illustrating regional bathymetric setting of the study area, marked by a star on Australia's Northwest Shelf. (c) Location map of the Torosa survey area (blue polygon) in the Browse Basin and regional 2D seismic lines (red). Location of line in part (d) is noted by the dashed blue line. (d) Regional stratigraphic setting, modified from Belde et al. [25]. Major surfaces (H4, H5, and H6) bound Carbonate Platform Phases (CPP-2, CPP-3, and CPP-4). ICP = isolated carbonate platform; SPB = seaward platform boundary; LPB = landward platform boundary. See text for discussion.

the South Asian Monsoon and the Australian monsoon ([11, 17–19]). These developments and the strengthened monsoon winds have been interpreted to have led to general intensification of ocean currents in both the Indian Ocean (Maldives; [8]) and South China Sea (Central Luconia; [11]).

To explore how architectural complexity of isolated carbonate platforms reflects the influences of these controls, this study examines the patterns of initiation, growth, and demise of platforms in a Miocene succession from the Browse Basin (Northwest Shelf, Australia). The results of mapping and dissecting over 100 platforms using high-resolution seismic data within a seismic stratigraphic framework reveal spatial and temporal trends in platform size, geometry, and seismic facies. These variations, compared to regional and global patterns, provide novel perspectives into the responses of carbonate reef and platform systems during the Miocene evolution of the Earth system. Results reveal sensitivity to paleoceanography, paleoclimate, and tectonics that may mask a global signal, a concept that may be broadly applicable to other carbonate platforms in the geologic record.

1.1. Geological Setting. The study area covers the extent of the Torosa 3D seismic survey on the Northwest Shelf of Australia (Figures 1(b) and 1(c)). Present-day depositional basins along this margin originated with Jurassic continental rifting associated with the breakup of Pangea. These early extensional phases developed a general NE to SW structural grain and a passive margin established by the Cretaceous.

Cenozoic history of the Northwest Shelf is marked by a pronounced northward drift of the Australian plate of roughly 20° latitude, from ~40°S in the Eocene-Oligocene to the subtropics today. This northward movement led to oblique collision between the Australian and Pacific plates and initiated counter-clockwise rotation during late Oligocene to early Miocene (Baillie et al. [20]). These movements led to the development of extensional faults, some of which reactivated older faults and some areas suffered structural inversion [21–24]. The Northwest Shelf today falls between 10°S and 22°S latitudes and includes the Northern Carnarvon, Roebuck, Browse, and Bonaparte basins.

Neogene carbonate strata of the Browse Basin have been the focus of numerous analyses in recent years [23–29]. These studies collectively have documented a regional long-term change from an Eocene-Oligocene cool-water carbonate ramp system that changed to a Miocene photozoan barrier reef-platform system, in part related to the northward drift of Australia from temperate to subtropical realms.

Regional exploration wells, including the Barcoo-1, Brecknock-1, and North Scott Reef-1 wells, were tied to seismic by several workers ([23–25]; no new data or ties are presented herein). These previous studies provide information on the ages of several key stratigraphic horizons (Figures 1(a) and 1(d)) from biostratigraphic, Strontium-age, and microfossil data. Mapping these horizons offers chronostratigraphic constraints on regional patterns of the Miocene part of the section, an interval documented to include several general phases. A first stage corresponds to the Aquitanian to Langhian Carbonate Platform Phase 2 (CPP-2) (Figures 1(a) and 1(d)), deposited between 17.5 and 15.1–14.5 Ma [25]. This stage included progradation and basinward growth of shallow-water carbonates. This growth and expansion led to establishment of a >500 km long barrier reef system with northern termination near the survey area, but which included a few isolated platforms landward of the barrier reef. A second stage, from the late Tortonian to the latest Messinian, included termination of the continuous barrier reef system, which then disintegrated into smaller, distinct isolated carbonate platforms. This stage includes the Langhian to Tortonian Carbonate-Platform Phase 3 (CPP-3), deposited between 15.1–14.5 and 9.8 Ma, and Carbonate-Platform Phase 4 (CPP-4) of Tortonian to Messinian age, younger than 11.1 Ma, but older than 4.08 Ma [25] (Figures 1(a) and 1(d)).

The numerous studies within the Browse Basin have resulted in several different seismic stratigraphic nomenclatural schemes, although most follow generally similar large-scale horizon correlations (recently summarized in [29]; cf. Figures 1(a) and 1(d)). This study follows the nomenclature of Belde et al. [25], who carefully described the first-order stratigraphic patterns on seismic in the area of focus herein. Their results provide the larger stratal framework for the more-detailed study of the platforms of the survey area (Figure 1(d)).

1.2. Seismic Data and Methods. This study documents stratigraphic patterns in the Torosa 3D survey, a high-resolution PSTM volume (*ca* 60 Hz in the Miocene part of the section) covering almost 800 km^2 (Figure 1(c)). The seismic data were acquired initially in 2005 and processed to zero phase, SEG reverse polarity (a downward increase in acoustic impedance forms a trough, red on the figures herein). The 1254 inlines have a spacing of 25.0 m, and the 3241 crosslines are spaced at 12.5 m. Regional information [28] suggests carbonate velocities in this interval of ~3400 m/s; this velocity and the dominant frequency suggest vertical resolution of ~15 m in the data. All estimates of thickness from isochron assume this velocity.

Seismic stratigraphic characterization facilitates subdividing the succession into genetically related architectural units. In the focus interval in this survey, surfaces discerned by stratal terminations such as toplap, onlap, downlap, and truncation were defined and carried consistently as far as the survey, their lateral extent, or data quality permitted, as troughs or peaks (e.g., assuming no change in phase) using Kingdom Suite software. Surfaces initially were picked on orthogonal grids with 10 or 20 line spacing, or less in local areas of complexity, then interpolated, checked, and reinterpreted at finer detail in heterogeneous areas as needed.

These surfaces provided a means to define stratal units bound by surfaces. Stratal units and surfaces were interpreted, characterized, and described in terms of time structure, unit isochron, internal geometries, qualitative seismic facies, and quantitative seismic attributes. These characteristics collectively define seismic units that separate the succession in the seismic volume into several packages.

Seismic facies describe subvolumes with distinct reflection character, as expressed based on distinct reflector amplitude, period, geometry, continuity, stacking, and position in

vertical profiles, or changes in time or horizon slices of amplitude, similarity, or other attributes. Seismic facies are defined based on objective and reproducible criteria [30], yet each can be interpreted in the context of geomorphic settings and environments of deposition. No core data through this interval are available to validate the interpretations with rock observations, however.

2. Results

Building upon the established regional stratigraphic framework [25], the focus here is on the application of seismic stratigraphy to describe and subdivide the sedimentary succession (summarized in a representative line in Figure 2). The subsequent analysis of the architecture and evolution of the suite of isolated carbonate platforms in the survey area [25, 31] utilizes this chronostratigraphic framework.

2.1. Seismic Facies and Stratigraphy. In the Miocene part of this volume, several seismic facies are ubiquitous throughout the succession (summarized in Figure 3). Beyond these common types, several unique facies occur in specific intervals or locations; as appropriate or useful, these distinct facies are described in later sections within their specific spatial and stratigraphic context. Each seismic facies includes distinct reflection amplitude, geometry, period, dip, continuity, and context, e.g., location within the succession, relative to other seismic facies (e.g., [30, 32]).

Seismic facies are illustrated and described in detail within the seismic stratigraphic framework; interpretations are below as well, as illustrated through the use of specific examples. These interpretations describe the general geomorphic setting that each seismic facies represents and are informed by, and consistent with, a previous work in the area by Saqab and Bourget [33], Belde et al. [25], and Van Tuyl et al. [28], and other Miocene examples (e.g., [32]). Nonetheless, there are no core data to validate the lithology or rock-facies interpretations.

2.2. Carbonate Platform Phase 2. Strata immediately older than those described here are part of CPP-2 (Figures 1(d) and 2(b)). This unit forms a pronounced northwest, basinward prograding shelf [25, 28, 29]. The terminal margin of this shelf lies in the northwest part of the survey (Figures 2(b) and 4(a)). This unit was not interpreted in any detail.

2.3. Carbonate Platform Phase 3. The lower carbonate succession considered here (CPP-3) includes three seismic units (LC-0, LC-1, and LC-2) named based on the surface that underlies them (Figures 2, 4, and 5). These units are subdivided by surfaces defined by toplap below and onlap above and are mappable across much of the survey. Although thicknesses of individual seismic units vary considerably, the succession as a whole is up to 0.212 s (360 m) thick (Figure 6).

2.3.1. LC-0. The basal seismic unit lies above the northwest-prograding clinoforms of CPP-2 (Figures 1(d) and 2(b)). To the northwest of this shelf-break of CPP-2, unit LC-0 is the thickest and it consistently exceeds an isochron of 72 ms (122 m) (Figures 4(a) and 6(a)). The seismic unit generally thins to the east and southeast (locally to less than 40 ms and 68 m). This unit includes a well-delineated, irregular eastern terminal margin (margin mapped as the red dashed line of Figure 6(b)) defined by abrupt thinning and onlap of overlying reflectors (e.g., green arrow, Figure 5(a)), but its western margin lies outside the survey area.

Internal seismic facies and geometries are quite varied. In areas of consistently thicker isochron, reflectors are of variable amplitude but include downlapping and irregular mounded geometries (Figures 4(c) and 5(a); seismic facies-(SF-) 5). In areas east of the terminal margin, high-continuity, low-amplitude parallel reflectors (Figures 4(c) and 5(a), SF-1) are interrupted by numerous isochron thicks (Figure 6(a)) of mounded reflectors that can include shingled clinoforms with roughly concentric reflectors in map view (Figure 5(b); SF-3 and 5; discussed in detail below). Locally, these mounded features occur at the isochron break (Figures 5, 6(a), and 6(b)).

2.3.2. LC-1. The basal reflectors of LC-1 onlap the previous northwest-oriented isochron thicks of LC-0 (Figure 5(a), green arrow). Above a basal reflector, areas to the east are dominated by low-amplitude, low-frequency continuous reflectors (SF-1), with scattered mounded, convex-up bodies with concentric reflectors (SF-5), some of which occur above, and expand the mounded features of LC-0 (Figure 5(b)). Isochrons approach 70 ms (119 m) in these downdip areas. To the west, SF-1 transitions abruptly laterally to thinner strata, generally less than 36 ms (61 m) thick. West of this transition occurs parallel, moderately continuous to bursty, moderate- to high-amplitude reflectors (SF-6) (Figure 5(a)). This well-defined isochron and seismic facies transition (Figure 4(c)), interpreted to represent the LC-1 shelf margin, is abrupt but irregular in map view and documents as much as ~8 km of eastward progradation from the LC-0 margin (compare Figures 6(b) and 6(c)), towards the intrashelf basin.

2.3.3. LC-2. The uppermost unit of the lower carbonate succession reaches up to 72 ms (122 m) thick (Figure 6(d)). The internal seismic character includes chaotic to low-amplitude, discontinuous parallel reflectors (SF-6) that sharply pass eastward into subtly mounded chaotic reflectors (SF-4) and inclined low-amplitude, high-similarity reflectors (SF-2) before transitioning into low to moderate amplitude, parallel to downlapping reflectors (SF-1) (Figures 5(a), 5(b), and 6(e)). These changes define an irregular but well-defined margin whose position locally is coincident with mounded features in the underlying seismic unit (Figure 6(f)), and this margin is onlapped by overlying reflectors (Figure 5(b), green arrow). Seismic unit LC-2 is the thickest in the area between its eastern, irregular margin, and the LC-1 margin and the thinnest above the mounded isochron thicks of the underlying units. This seismic unit does not appear to include any smaller mounded features with circular map view patterns, but represents the eastward shift of the shelf margin of the barrier reef ("landward platform boundary" of [25], cf. Figure 1(d)). Thus, relative to the margins of LC-0 and LC-

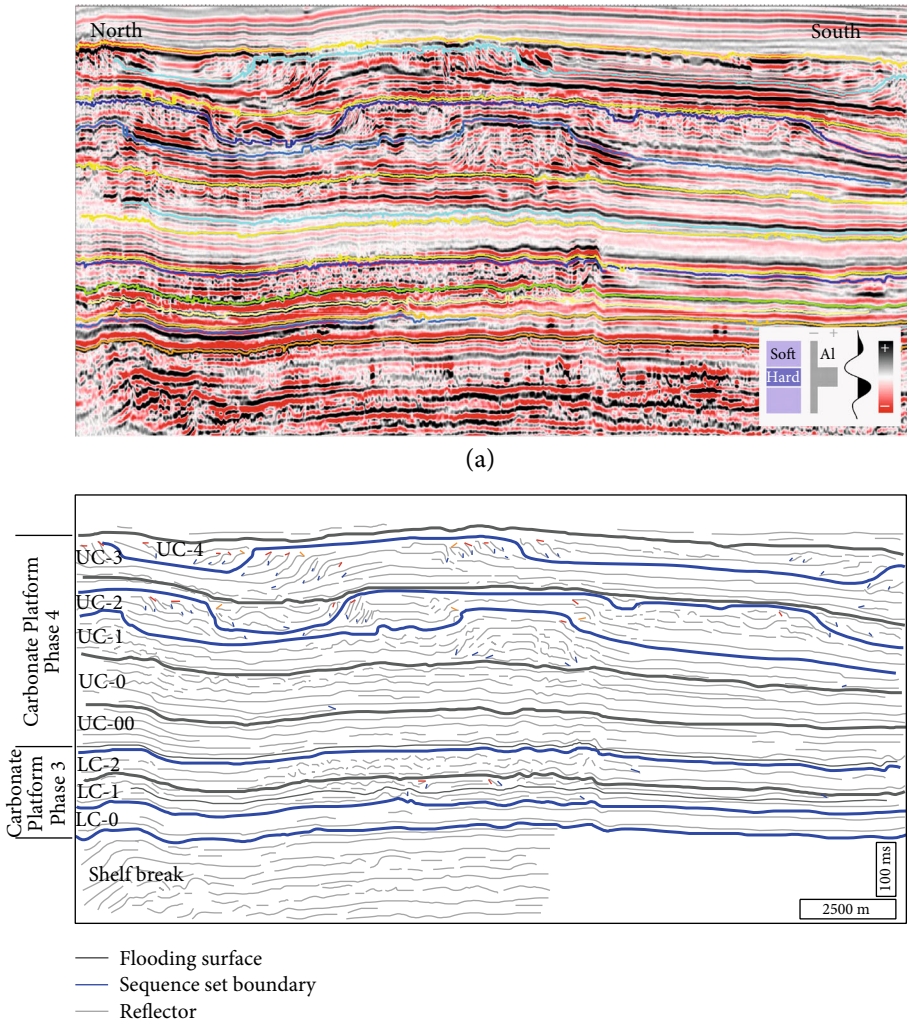

FIGURE 2: Seismic stratigraphic framework, illustrating distinct changes in isochron and seismic character that define isolated platforms. (a) Interpretations on a seismic line from the Torosa survey and (b) interpretive sketch diagram. In the latter, tics note key stratal terminations: blue = downlap, red = toplap, and orange = onlap. See text for discussion.

1, the shelf margin of LC-2 stepped further landward into the intrashelf basin (Figure 6(f)). Patchy circular, high-amplitude features are ubiquitous on the upper surface (UC-00), and this horizon also includes several sinuous, branching features (Figures 6(g) and 6(h)).

2.4. Carbonate Platform Phase 4. The upper carbonate succession corresponds to CPP-4 of Belde et al. [25] and includes six seismic units (UC-00, UC-0, UC-1, UC-2, UC-3, and UC-4) (Figures 1(d) and 2). Each unit has distinct stacking patterns, and they are defined by basal onlap or downlap and surfaces of toplap (above), as discussed above (cf. Figure 2). This succession as a whole is up to 470 ms (794 m) thick.

2.4.1. UC-00. This seismic unit is of generally consistent isochron of ~72 to 92 ms (122 to 156 m) throughout most of the area. In the east of the previous (LC-2) shelf margin, it is thicker due to the basal onlapping units, and its isochron reaches up to 142 ms (241 m) in those areas. In low to moderate amplitude, parallel continuous seismic facies (SF-1) are most common this interval (Figures 2 and 5(c)), although one subtle oblong isochron thick is evident in NW extremity of the survey.

2.4.2. UC-0. A surface of downlap defines the base of this seismic unit, and it includes seismic facies very similar to those of UC-00. The unit includes one circular mounded feature ~2.5 km across and up to 50 ms (85 m) relief (defined by time relief of inclined reflectors within SF-2) and a few NE-SW elongate, low-relief mounded features with amplitudes higher than the surrounding areas.

2.4.3. UC-1. Seismic unit UC-1 varies markedly in isochron and seismic facies. In general, isochron thicks (up to 142 ms, 241 m) form broadly circular, convex-up features (Figure 7, lower slice) that include cores of low-amplitude discontinuous to chaotic reflectors (SF-5 near the base, SF-4

Seis. facies	Amplitude	Geometry	Continuity	Associations	Interpretation
SF-1	Low to moderate	Continuous, parallel to low-angle downlapping	High similarity	Downdip of SF-2, SF-3 or SF-4	Basin
SF-2	High to moderate	Offlapping oblique to less commonly sigmoid, create along-strike subparallel bands	Very low across strike, high to variable along strike	Updip of SF-1; Downdip of SF-4 SF-5	Slope
SF-3	High to moderate	Toplap and downlap	High similarity	Updip of SF-1; Downdip of SF-4 SF-5	Slope
SF-4	Low to moderate	Chaotic	Low similarity	Updip of SF-1 or SF-2, lateral to SF-6	Reef
SF-5	Low to high	Mounded, convex-up parallel to toplapping	High similarity	Updip of SF-1 or SF-2, lateral to SF-6	Reef to platform
SF-6	Variable–low to high, commonly bursty	Chaotic to parallel continuous to low-angle toplap	Low to moderate similarity	Common in isochron thicks, updip of or adjacent to SF-4, SF-5	Platform interior

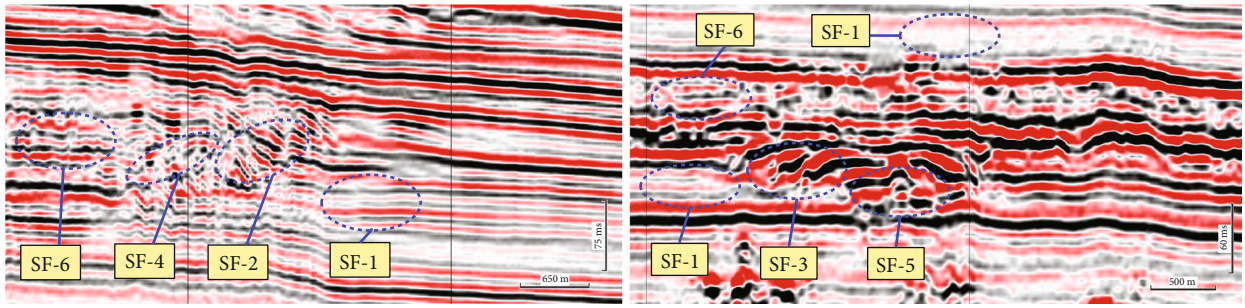

Figure 3: Summary of seismic facies, middle and upper Miocene strata, and Torosa survey area. Detailed examples and interpretations are documented below in the text and figures.

and SF-6) (Figure 5(c)). These seismic facies pass laterally outward to inclined, parallel, toplapping (updip), and downlapping (downdip) reflectors (SF-2), which in turn pass to a thinner succession of parallel, broader, generally continuous reflectors (SF-1) between isochron thicks (Figures 5(c) and 7). These thin areas are generally less than 60 ms (102 m) thick.

2.4.4. UC-2. Seismic unit UC-2 forms a succession up to 92 ms (156 m) thick. A basal succession forms reflectors that onlap the flanks of the isochron thicks of UC-1, some of which represent flat-topped to offlapping terraces (Figure 5(c)). These reflectors pass downdip into parallel continuous to downlapping, low-frequency reflectors (SF-1) (Figure 5(c)) or wavy, variable amplitude reflectors in some lows between previous isochron thicks. Above this basal unit, seismic facies are broadly similar to those of UC-1. Positions above the previous thicks and highs of UC-1 include almost exclusively variable amplitude, parallel reflectors (SF-6) (Figure 5(c)). These reflectors extend in extent and pass into inclined, oblique to (less commonly) sigmoidal clinoforms (SF-2), many of which downlap the basal succession (Figure 5(c)). Collectively, the highs follow the same trends as UC-1 but expand up to 8 km in lateral extent by progradation and infilling previous lows (Figure 5(c) and 7, middle slice). The upper surface of this unit is defined by toplap of underlying units and onlap of overlying reflectors.

2.4.5. UC-3. The basal strata of seismic unit UC-3 onlap the highs of UC-2 and are overlain by a continuous downlap surface (Figure 2). This basal package of strata reaches up to 92 ms (156 m) and largely fills the lows between the highs of UC-2 (Figure 2). The upper part of this seismic unit, above the downlap surface, is up to 152 ms (258 m) thick and is marked by two elongate isochron thicks. The seismic facies are isochron thicks of parallel, aggradational to backstepping, moderate to high amplitude reflectors (SF-6) that pass laterally to moderate amplitude, highly progradational toplapping, and downlapping reflectors that form oblique, sigmoidal, to shingled clinoforms (SF-2) (Figure 2). These features in turn pass outward and downdip, downlapping into thinner, moderate amplitude, parallel, continuous reflectors (SF-1) in the lows. The upper surface of this interval is defined below by toplap and above by onlap of the UC-3 thicks, but it is downlapped in basinal locations (Figure 2). Although the seismic facies and the presence of isolated

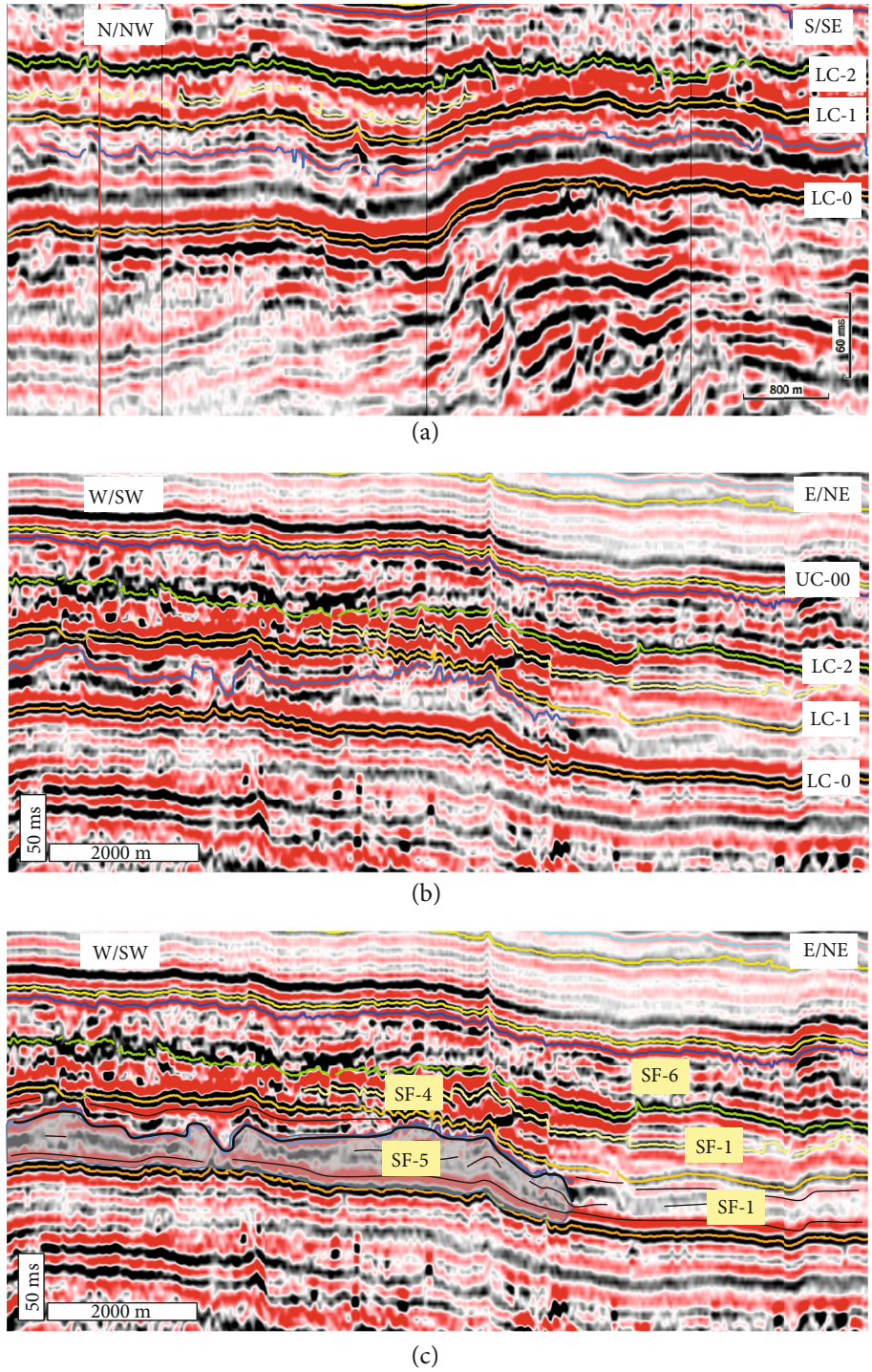

FIGURE 4: Seismic character, Carbonate Platform Phase 3. (a) Representative seismic line. Note the pronounced CPP-2 shelf break below LC-0 and thinning of strata above, notable in LC-0 and LC-1. (b) Illustrative seismic line and (c) the same line annotated with seismic facies (SF). Note the mounded geometries (SF-5) in the lower seismic unit (greyed out) and the lateral changes in LC-1 to SF-1 towards the east/northeast.

isochron thicks are broadly similar to UC-1 and UC-2, their size, shape, and locations are quite distinct from those units (Figure 7, upper slice).

2.4.6. UC-4. Seismic unit UC-4 is up to 88 ms (150 m) thick and largely fills the lows between the mounded highs of UC-3 and onlaps those highs (Figure 2). On top of those highs, this succession may be 20 ms or less (<34 m) in thickness. Seismic facies are quite varied and range from toplapping and downlapping reflectors of shingled to oblique clinoforms (SF-2), to parallel moderate amplitude, continuous reflectors (SF-1) in the lows. In two areas, high amplitude, parallel continuous reflectors (SF-6) that collectively form an ovoid pattern in map view pass laterally to low to

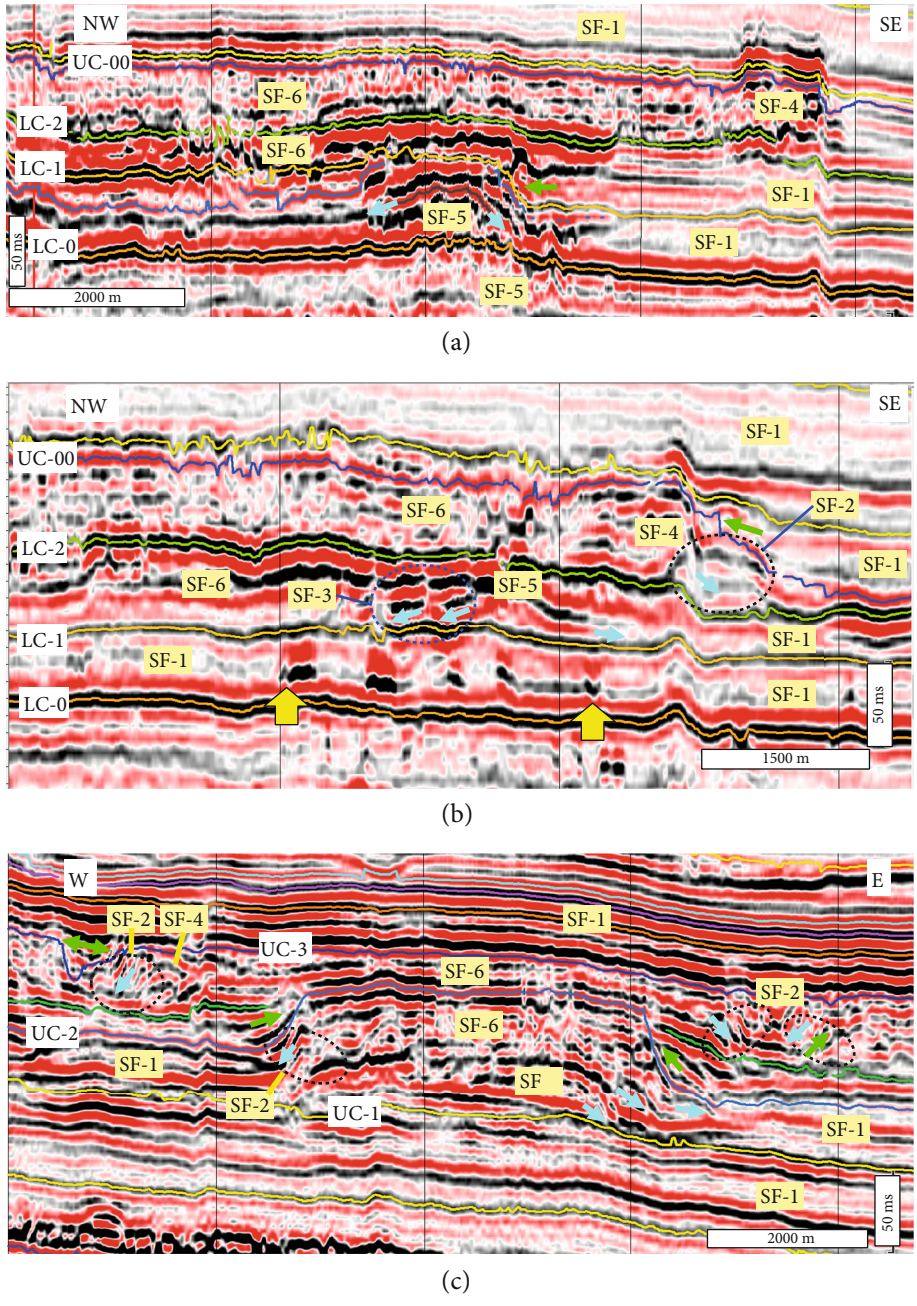

Figure 5: Illustrative lines documenting seismic character and seismic facies, Carbonate Platform Phases 3 and 4. (a) Seismic line showing a mounded geometry in LC-0, thickening and changes in seismic character to the SE of this feature in LC-1, and well-defined shelf margin in LC-2. Green arrow emphasizes onlap onto the LC-1 surface. (b) Representative seismic facies in CPP-3. High amplitude bursts between yellow arrows in LC-0 form circular features to ovoid features in map view. In LC-1, the downlaps (blue arrows) form roughly concentric features in map view. Blue arrows illustrate downlaps, and green arrow highlights onlap. (c) Representative seismic facies in CPP-4. Blue arrows illustrate downlaps, and green arrow highlights onlap. See text for discussion.

moderate amplitude, toplapping reflectors (SF-2) that downlap onto SF-1 of the underlying seismic unit (Figure 2; these features are documented in detail below). These strata include clinoforms that progressively fill the lows. The succession is capped by a regional surface of downlap, which is in turn overlain by reflectors of SF-1.

2.5. Interpretation: Seismic Facies and Seismic Stratigraphy. Each seismic unit is bound by surfaces of downlap or onlap at their base and toplap at their top. Across these surfaces, there commonly is a pronounced change in seismic character, such as variable amplitude, similarity, or progradation direction. Aside from terminations that define their base and top, several units include one or more internal downlap surfaces (Figure 2). These seismic units thus are interpreted to represent composite sequences; several of these seismic units (especially in CPP-4) include sequence sets of more than one distinct seismic sequence with discrete stacking

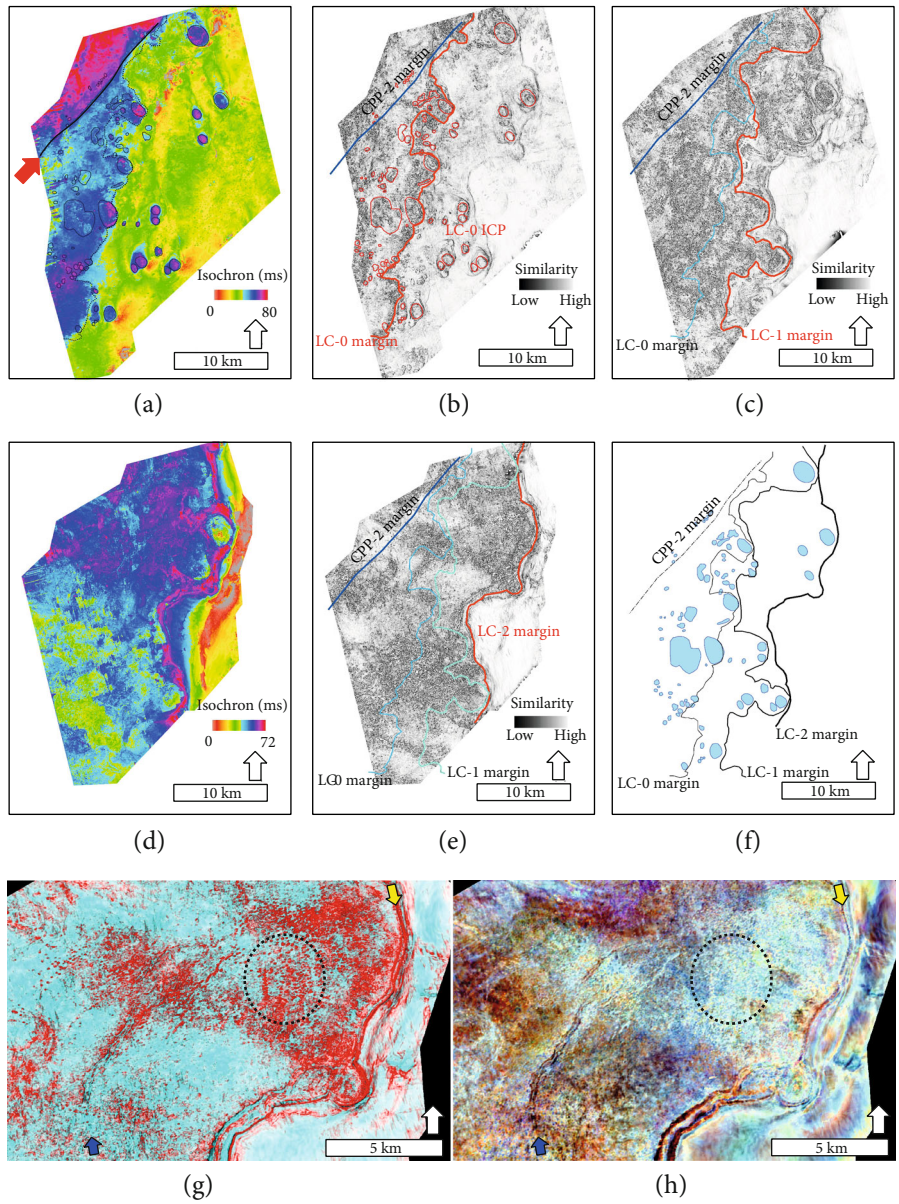

Figure 6: Spatial patterns of Carbonate Platform Phase 3. (a) Isochron LC-0. Note a thicker interval northwest of the shelf break in CPP-2 (solid line, that shelf was prograding to the NW; cf. Figures 1(c) and 2, [25]). The data also reveal isolated thicks to the east. (b) Similarity map, surface LC-1 (e.g., top of LC-0). Blue line is the previous (CPP-2) margin. The bold red line highlights areas with marked isochron shift, interpreted as the landward shelf margin, and red circles emphasizes margins of isolated platforms (ICP). (c) Similarity map, surface LC-2 (e.g., top of LC-1). Blue line is LC-0 shelf margin from part (b). Red line highlights areas with marked isochron shift, interpreted as the landward shelf margin. The margin of seismic unit LC-0 is included as the blue line for reference. (d) Isochron LC-2. Note a thicker interval bounded to the east by a marked thinning. (e) Similarity map, top surface of LC-2. Red line highlights areas with marked isochron shift, also accompanied by changes in similarity, interpreted as the landward shelf margin. Margins of seismic units LC-0 and LC-1 are included as blue lines for reference. (f) Map summarizing the position of shelf margins (black lines) and isolated platforms (blue polygons). Following deposition of the northwest-prograding CPP-2 shelf margin, the shelf margins of CPP-3 represent irregular but persistent eastward progradation. (g, h) Map of RGB blend of (g) amplitude (red) and similarity (green and blue) and (h) 48-62-80 Hz spectral components at top LC-2 surface. These plots document numerous high-amplitude patches (e.g., dashed oval), the terminal shelf margin (yellow arrow; compare SF-4 of Figure 5(a)), and an irregular sinuous feature (blue arrow). See text for discussion.

patterns. These individual, higher-order sequences are documented within individual platforms in detail below.

Collectively, the patterns of CPP-3 are interpreted to represent the initiation of isolated carbonate platforms and their gradual expansion and growth, across the shelf. Seismic unit LC-0 reflects the initiation of numerous isolated platforms and a subtle, low relief shelf in the west third of the survey (Figures 4 and 5). Similarly, seismic unit LC-1 represents continued growth of many outboard (eastern) platforms and a gradual progradation of the shallow shelf towards the

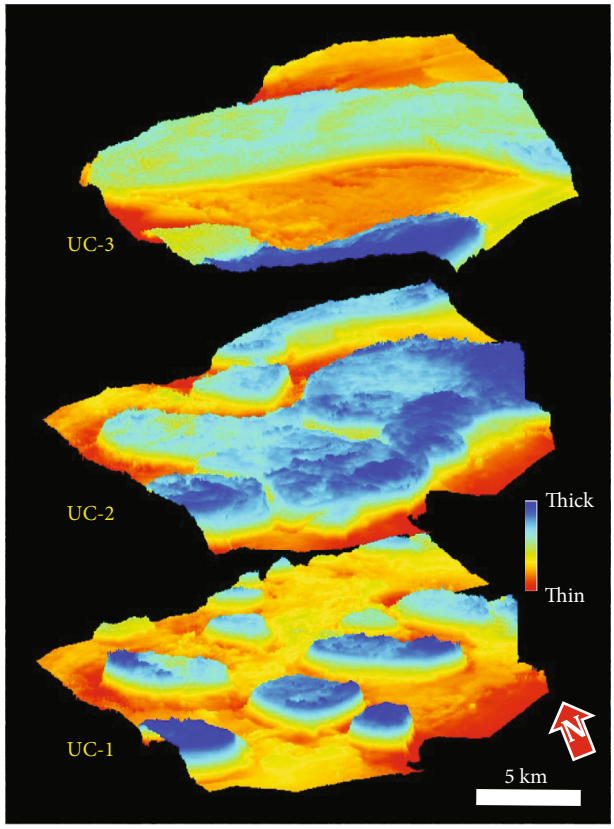

FIGURE 7: General patterns of platform growth, illustrated by isochron maps. Lower surface (UC-1) is isochron of UC-1, middle surface (UC-2) is isochron on UC-1 + UC-2, and upper surface (UC-3) is isochron from a marked downlap surface (UC-3fs) to UC-4. Note that the platforms that nucleated in UC-1 grew and expanded during deposition of UC-2 but include markedly distinct trends in UC-3.

east. Progradation is most pronounced in areas with preexisting platforms (compare patterns in Figures 6(b) and 6(c), locations of shelf margins in Figure 6(f)). Many of the LC-0 platforms were covered and form promontories in the irregular LC-1 shelf margin (Figure 6(f)). Seismic unit LC-2 represents continued, but irregular, eastward progradation of the shelf margin and establishment of a broad, flat-topped shelf that passes eastward into a deeper slope and intrashelf basin. The circular features (Figure 6(g)), coupled with the sinuous branching form (Figure 6(h)), are suggestive of karst at the top of this succession.

CPP-4 includes two basal seismic units (UC-00 and UC-0) with thick successions of moderate amplitude, parallel to low-angle downlapping reflectors (SF-2) and only a few mounded features (SF-5 and SF-6) (Figure 5(c)). These strata are interpreted to represent a flooding interval, with limited areas of shallow-water carbonate production. UC-1 is characterized by initiation and growth of several small platforms. A pronounced lowstand (e.g., surface UC-2), suggested by the onlapping terraces, also nucleated some platforms within interplatform areas. Following reflooding of the platform tops, they expanded considerably in unit UC-2 (Figure 7). The markedly different geomorphic patterns of the platforms and interplatform seaways within UC-3 suggest a pronounced geomorphic reorganization. UC-4 strata represent nucleation of several new isolated platforms and expansion of the UC-3 platforms, both of which gradually infilled parts of the interplatform seaways. Ultimately, the succession is capped by a thick interval of parallel to low-angle downlapping reflectors (SF-1) (Figure 2(b)), interpreted to represent termination of the platforms and pronounced flooding.

2.6. Spatiotemporal Changes of Geometry and Architecture of Isolated Platforms. Seismic stratigraphy subdivides the section into several genetically related units. These stratigraphic units provide the basis for interpreting the geometry, architecture, and seismic geomorphology of isolated platforms throughout the succession. The results reveal marked changes in space and time.

2.6.1. Carbonate Platform Phase 3. The basal reflectors of LC-0 across the survey area include several hundred small circular features, many <400 m across, evident on time and horizon slices of amplitude and similarity (Figures 5(b), 8(a), and 8(b)). These features include no clear evidence of internal geometry, occur near the base of the composite sequence, and are downlapped.

Of these several hundred initial diminutive features, roughly 80 persist above the basal reflectors and expand to greater than 0.016 km^2 in size (e.g., Figures 5(a) and 5(b)). These platforms are focused in a NE-SW-oriented trend where the present-day structure highly intersects the previous shelf margin, although a few form isolated platforms to the east, in the intrashelf basin. They reach up to 9.3 km^2 in size (mean = 0.6 km^2) and relief of several platforms approach 80 m. Isolated platforms include cores with concave-down parallel reflectors (SF-5), flanked by inclined, toplapping reflectors (SF-3) that commonly form circular to ovoid features in time slices (Figure 8(c)). Asymmetry and platform elongation is associated with lower angle or extra reflectors and can be subtle (Figures 8(c) and 8(d)) or pronounced (Figures 8(e) and 8(f)). Most frequently, elongation occurs towards the north to northwest or west, away from the deeper-water intrashelf basin and generally towards the open Indian Ocean.

In seismic unit LC-1, the isolated platforms of LC-0 were either covered and subsumed by the expanding shelf (64), expanded (7), or expanded and amalgamated with nearby platforms (4 sets) (Figures 9(a)–9(d)); six new platforms initiated in different locations (cf. Figure 6(b)). The maximum size of resulting 18 distinct, mappable platforms in LC-1 is 6.18 km^2 (mean = 1.8 km^2). These isolated platforms that lie outboard of the LC-1 shelf margin include onlap onto the flanks of LC-0 platforms, followed by aggradation and progradation with sigmoidal to oblique clinoforms (Figures 9(a) and 9(c)). As in the larger platforms of LC-1, expansion most commonly occurred towards the northwest, with more common and lower-angle reflectors in that direction; up to 1 km of progradation occurred (Figures 9(b) and 9(d)). The tallest platform included 56 ms (95 m) of syndepositional relief.

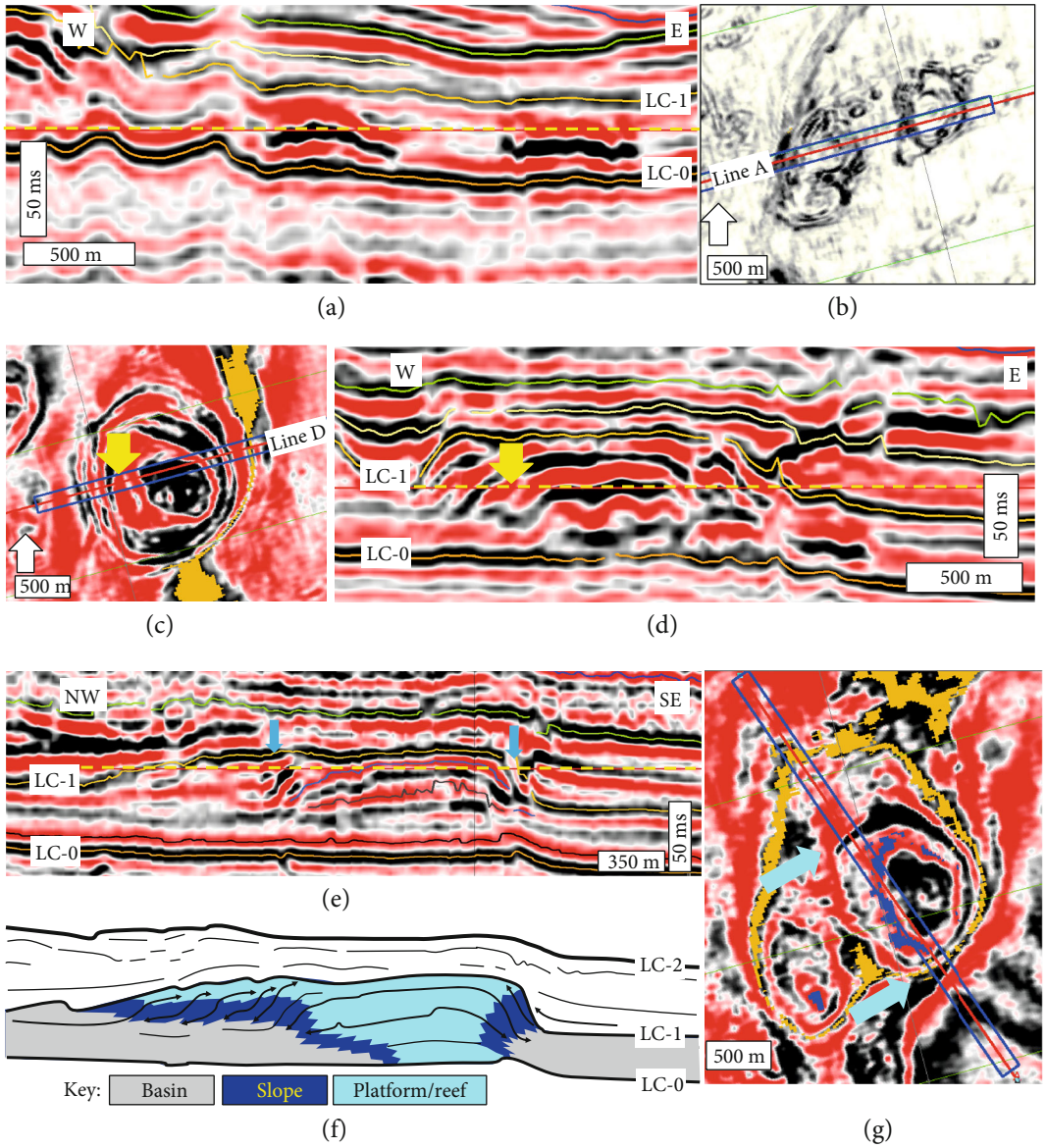

FIGURE 8: Seismic character of selected platforms, Carbonate Platform Phase 3. (a) Seismic line illustrating amplitude bursts in unit LC-0. (b) Map view of semblance time slice across these amplitude bursts, at the level of dashed yellow line. In this and subsequent amplitude or similarity maps, the red lines bound by blue polygon on maps mark the location of the associated seismic line. Note the two circular to ovoid platforms that correspond to the amplitude bursts. Amplitude time slice (c) and seismic line (d) through a mounded platform in unit LC-0. Amplitude time slice is at the level of yellow line in part (d). Yellow arrows highlight a reflector present only on the west and northwest side of the platform. Seismic line (e), interpretive sketch diagram (f), and amplitude time slice (g) through a LC-0 platform. Time slice is at the level of yellow line in part (e). Note the elongation and the progradation that is more pronounced to the north-northwest than other directions.

Seismic unit LC-2 represents deposits of a broad, shallow shelf that continues for several km west of the survey area (Figures 1(c), 5, and 6) [25]. As such, no separate isolated platforms that stood with marked relief are evident in the survey area.

2.6.2. Carbonate Platform Phase 4

(1) UC-1 Platforms. Seismic units UC-0 and UC-00 include dominantly low- to moderate amplitude, parallel to downlapping reflectors, but with very few low-relief mounded features. As a result, the deposits of UC-1 represent the next seismic unit with numerous isolated carbonate platforms. The patterns of time at top of the seismic unit define 13 platforms, of which 7 fall completely within the study area (Figure 7, lower slice). These platforms range in size up to 25 km^2 and include up to 98 ms (167 m) of relief; at the largest scale, most are broadly elongated NW-SE.

(a) Platform A. The internal architecture of the UC-1 platforms varies considerably. For example, one platform started with a subtle isochron thick in a basal succession (below S1 in

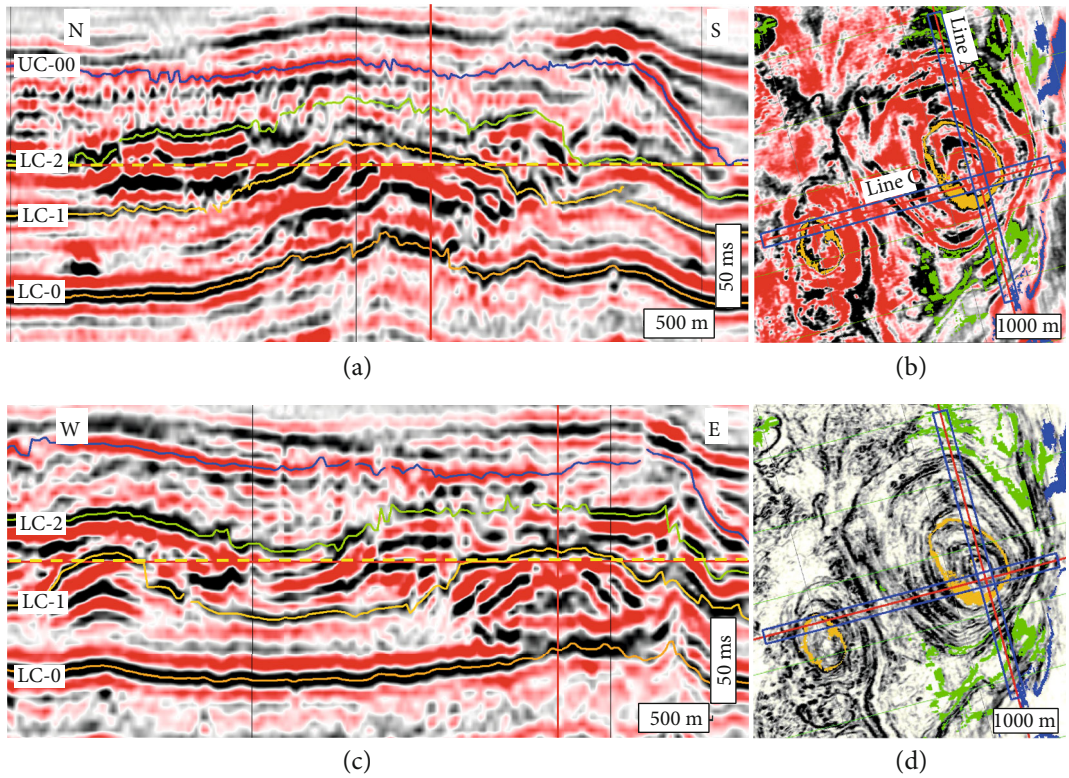

FIGURE 9: Seismic character of representative platforms, Carbonate Platform Phase 3. (a) Seismic line through a platform. (b) Amplitude time slice through platform. Parts (a) and (b) show that the platform starts in LC-0 but continues to expand and grow through LC-1. The LC-2 shelf margin occurs just south of this area, as is evident in the seismic line. (c) Seismic line through the same platform, and a smaller platform to the west. (d) Semblance time slice through platforms. Note the northwest elongation. Time slices are at the level of yellow line in parts (a) and (c).

Figure 10(a)), which manifests as two peak-trough loops in some areas. The isochron of this interval is up to ~32 ms (54 m), and it is downlapped by overlying units. The second unit (between S1 and S2 in Figure 10(a)) defines a broad oval that covers 3.2 km^2, roughly corresponding to the area inside the bright green (Figure 10(b)). It includes several smaller thick areas with an extra upper loop and an isochon up to ~36 ms (61 m), with approximately 20 ms (34 m) relief on its flanks. The third unit (between S2 and S3) includes a pronounced area of thick isochron that is elongated W/NW to E/SW (long axis ~110°; evident in the area encircled by dark green in the time slice of Figure 10(c)). It covers an area roughly 2.5 × 1 km on top of, but smaller than, the previous high. The thickest area includes an isochon of up to ~36 ms (61 m) and relief of roughly 28 ms (48 m). This surface is downlapped by clinoforms of the overlying unit, between S3 and UC-2 (Figure 10(d)). This uppermost unit includes parallel, aggradational to offlapping reflectors, with most pronounced progradation (in excess of 750 m) in a subtle embayment on the northern part of the thick. It is capped by UC-2, a surface of toplap in areas of thick isochron, which is in turn onlapped on flanks of the thick isochron (Figures 10(a) and 10(d)). Isochron of this UC-2 thick defines a mounded feature roughly 2.2 × 2.9 km that covers an area of 4.5 km^2 (enclosed by the blue UC-2 horizon, Figure 10(c)), an isochon that reaches up to ~48 ms (82 m), and syndepositional relief of at least 32 ms (54 m) (Figures 10(a) and 10(d)). Isochron is thinner above the underlying elongate mound and thickest off its flanks in the area of the clinoforms.

(b) Interpretation. This succession is interpreted to represent an isolated carbonate platform with three growth phases (red triangles of Figure 10(d)). The platform expanded laterally in the basal two phases, separated by surfaces (S1 and S2, Figure 10(d)) and gradually increased in relief. Following a backstep to a less aerially extensive platform and a downlap surface (S3, Figure 10(d)), the uppermost platform phase expanded to about the same size as the basal two phases by progradation above S3. Capped by surface UC-2, this final phase included greater syndepositional relief and gradients and pronounced progradation before termination.

(c) Platform B. A second, nearby UC-1 platform illustrates some similarities and some differences (Figure 11). This platform started as three-kilometer scale mounded features (Figures 11(b) and 11(c)) with an extra internal reflector, capped with horizon R1, which is downlapped by younger strata (Figure 11(f)). Of these features, the smaller two (2.7 and 1.5 km^2) are elongated, with azimuths of 110 and 125°, similar to the first platform; the third one (3.3. km^2) is more equidimensional (Figures 11(b) and 11(c)). This unit has up to 60 ms (102 m) thickness, and its upper surface has between 32 and 40 ms (54 to 68 m) of gentle relief. A middle unit

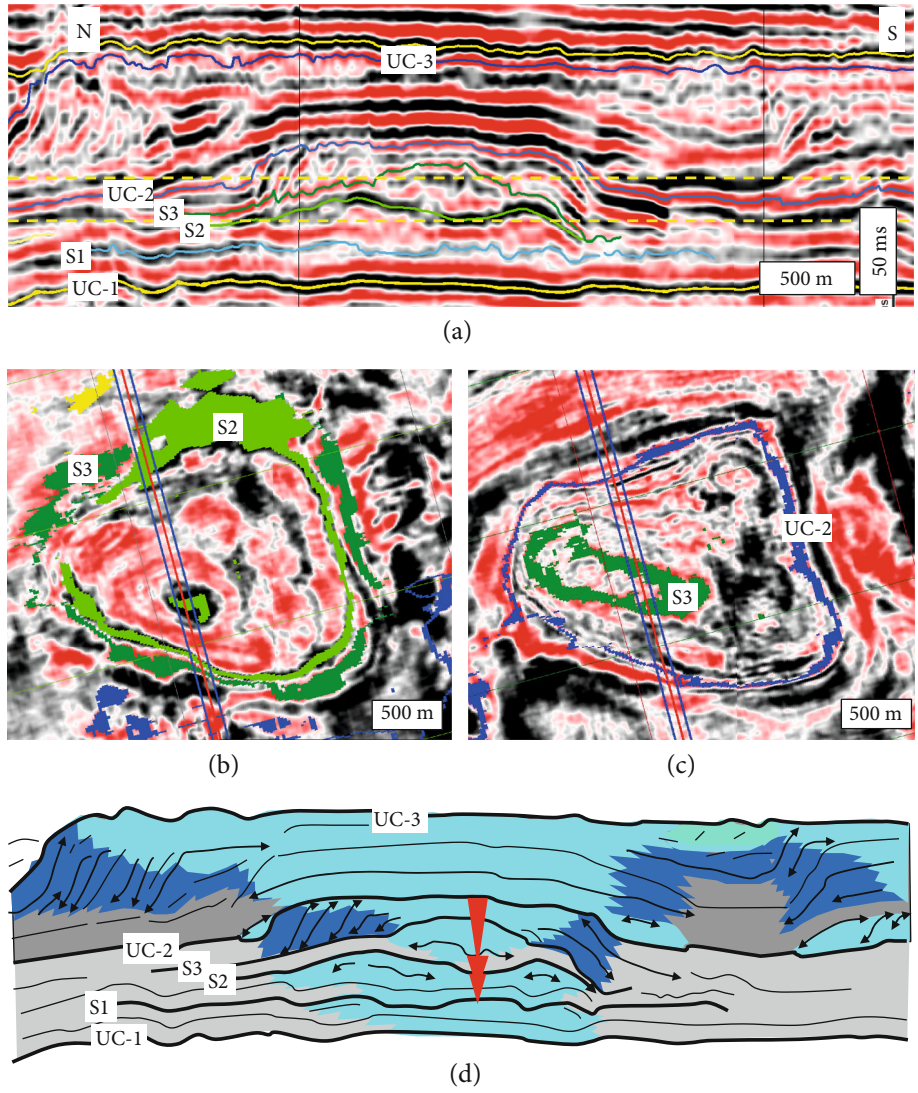

FIGURE 10: Seismic character of a representative platform, Carbonate Platform Phase 4. (a) Seismic line through an illustrative UC-1 platform. Position of time slices indicated by dashed yellow lines. (b) Lower amplitude time slice through the platform. Note the broad ovoid platform defined by S2. (c) Upper amplitude time slice through the platform. Note the narrow west-east elongate platform outlined by S3, of much less lateral extent than the S2 platform. The upper stage, capped by surface UC-2, appears roughly the same extent as the lower-relief S2 platform. (d) Interpretive sketch diagram of platform growth. Red triangles indicate the three seismic sequences discussed in the text. Colors of interpreted geomorphic elements are as noted in Figure 8(f). Note how the platform growth trend continues from UC-1 to UC-2. See text for detailed discussion.

includes aggradational to progradational geometries that largely fill lows among the three mounds (Figure 11(d) and 11(e)), capped by a surface of toplap (horizon R2), and which is also downlapped and onlapped by reflectors of the upper unit (Figure 11(f)). This middle unit forms a broad mounded feature of 16 km^2, with an orientation of roughly 110°. This unit includes at least 48 ms (82 m) of relief on its well-defined margins, and it is up to 56 ms (95 m) thick, thickest on the flanks of paleo-highs of the lower unit. Above basal onlapping reflectors, the capping unit is characterized by aggradational to progradational geometries (Figures 11(a) and 11(f)). It is overlain by a surface with local toplap (horizon UC-2) which also is onlapped on the flanks of the isochron thick (Figures 11(a) and 11(f)). The unit progrades most markedly in a southwest-facing embayment, but around most of the area, its terminal margins are roughly coincident with those of the underlying succession (Figures 11(a) and 11(f)). This unit is up to 88 ms (150 m) thick and includes up to 52 ms (88 m) relief on its upper surface. In total, at the time of termination (surface UC-2), this feature includes a total thickness of 142 ms (241 m) and covers 17 km^2.

(d) Interpretation. These observations are interpreted to reflect the growth of an isolated carbonate platform (Figure 11(f)). An initial cluster of three small, broad, low-relief platforms gradually coalesced and built up into one larger platform. Although it too consists of three units

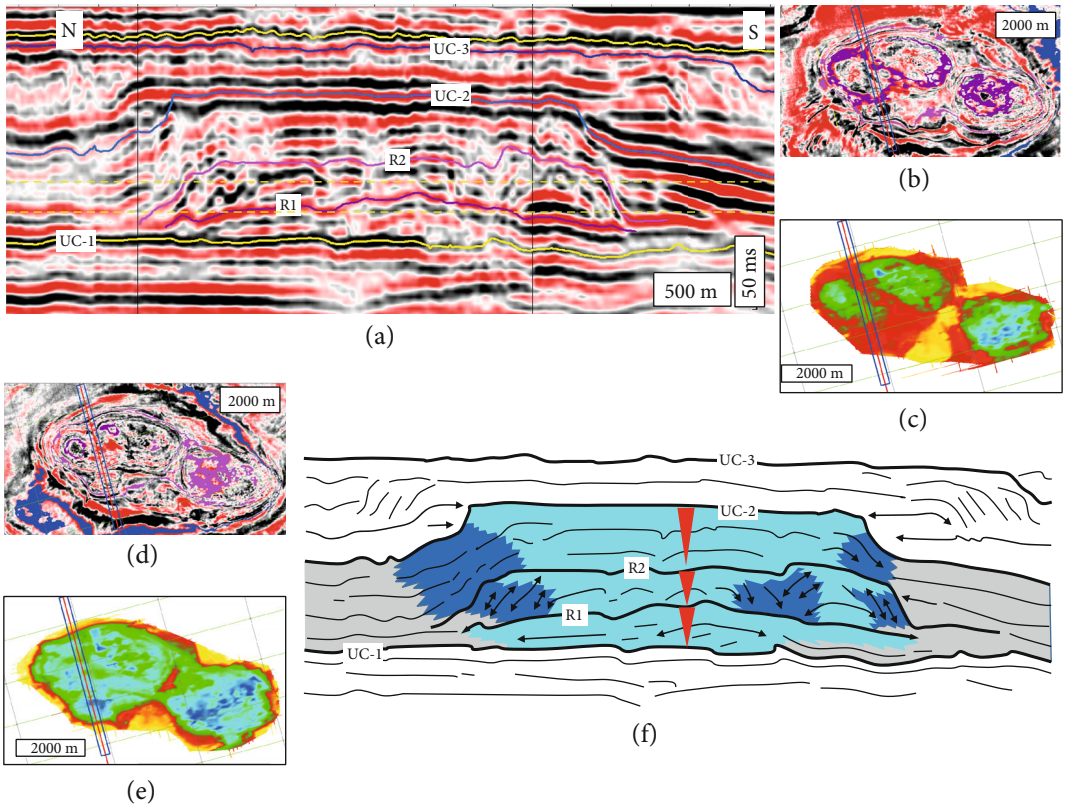

FIGURE 11: Seismic character of a representative UC-1 platform, Carbonate Platform Phase 4. (a) Seismic line through the platform. Position of time slices indicated by dashed yellow lines. (b) Amplitude, lower time slice. Note the three elongate ovoid platforms with generally radial growth. (c) Time, horizon R1, identifying three small platforms. (d) Amplitude, upper time slice. (e) Time, horizon R2. Note that the platforms have merged. (f) Interpretive sketch diagram of platform growth. Colors of interpreted geomorphic elements are as noted in Figure 8(f). Red triangles indicate the seismic sequences discussed in the text.

subdivided by downlap surfaces, unlike the previously described platform, this platform did not include a middle backstepped phase (compare Figures 10(d) and 11(f)). The third capping phase did not markedly expand the platform, except by progradation in an embayment to the southwest.

(e) Platform C. A third platform also illustrates three growth stages but has distinct stratal patterns. A basal unit (between UC-1 and H1; Figures 12(a) and 12(b)) includes two areas of concentric rings in amplitude time slices (Figure 12(c)) that broaden and converge outward. In vertical sections, this interval is up to 56 ms (95 m) of low-amplitude, low continuity reflectors. Surface H1 defines a broad, elongate mound up to 0.8 × 2.5 km long that covers 1.6 km^2, with a long axis with an orientation of ~112°. Above surface H1, the basal strata of the middle unit onlap the flanks of the thick and form low-relief clinoforms that progressively step downward (right side of Figure 12(a)). These reflectors and an overlying parallel, horizontal reflector are capped with a horizon (H1dls) that can be mapped across the area and through the platform (Figures 12(a), 12(b), and 12(e)). This reflector is in turn downlapped by clinoforms that also toplap into surface H2 (Figure 12(e)). The strata between H1dls and H2 are thin, mostly less than 24 ms (41 m), but reach up to 40 ms to the west and north of the thick defined by H1, in areas with clinoforms (Figure 12(a)). The high of H2 defines an elongated mounded feature extending to an area of 2.1 km^2 (Figure 12(d)). The upper unit between H2 and UC-2 is thin (<20 ms and 34 m) except in areas of inclined reflectors, where it reaches up to 42 ms (71 m). As in the other examples, surface UC-2 is toplapped below (left side of Figures 12(a) and 12(e)) and onlapped by younger strata. It defines a high that is broader than that of the underlying units, with expansion to the north and northwest of up to 0.5 km, and a high that covers an area of 2.8 km with up to 60 ms (102 m) of relief.

(f) Interpretation. The internal seismic architecture of this feature is interpreted to represent three phases of growth of an isolated platform system (Figure 12(e)). Two initial, smaller low-relief mounds aggraded and merged, creating a larger isolated platform. The downward-stepped clinoforms on the flanks of this succession are interpreted to represent a relative fall in sea level. The H1 platform and these flanks are overlain by a correlatable surface of downlap (H1dls), interpreted as a flooding surface. Above H1dls, a second platform phase nucleates and expands somewhat to the north and northwest. This pattern of aggradation over the previous high, and north-northwest progradation, continued in the third phase of this platform.

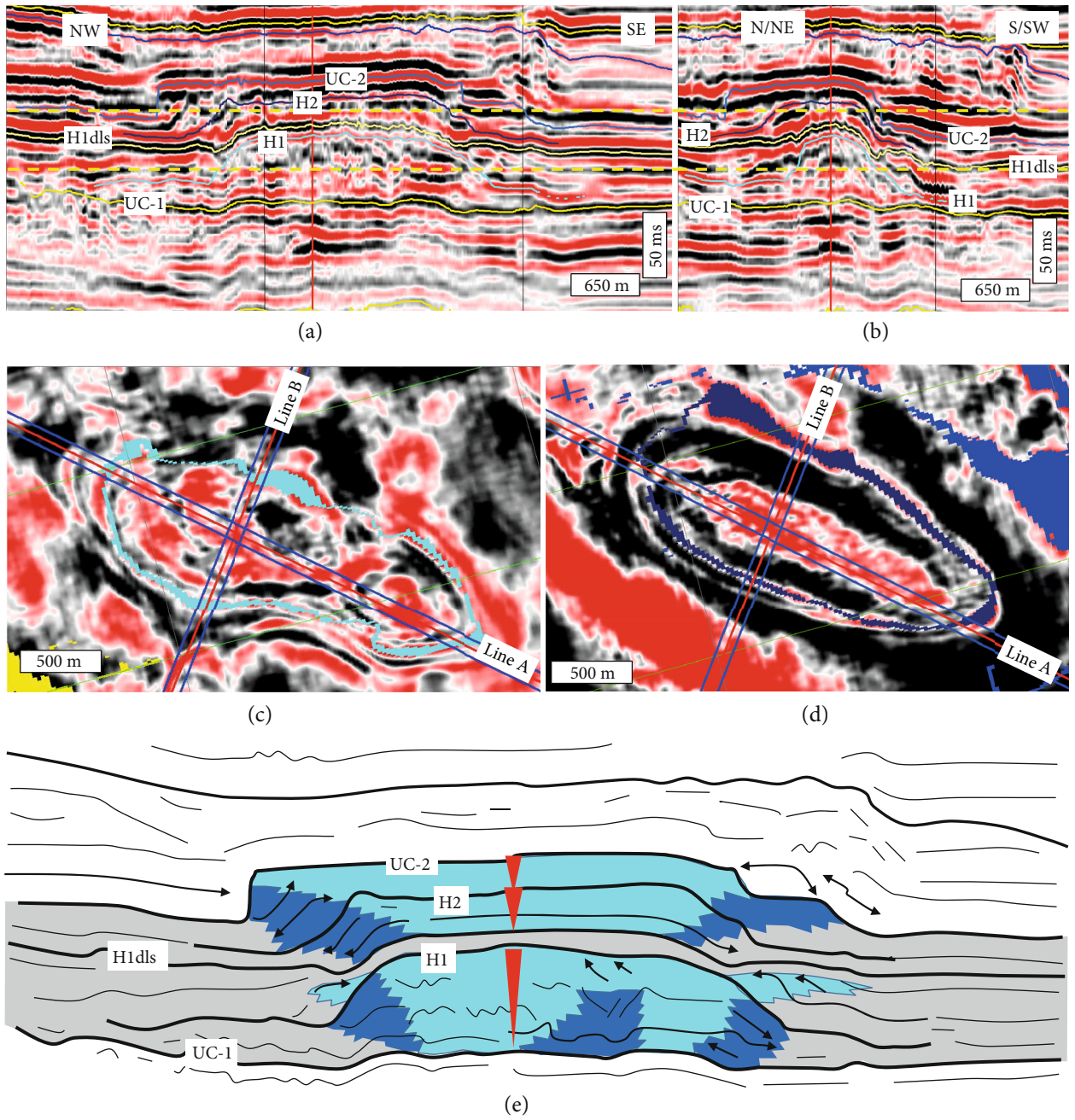

Figure 12: Seismic character of an illustrative UC-1 platform, Carbonate Platform Phase 4. (a, b) Seismic lines through the platform. Line locations are normal to one another, as indicated in parts (c) and (d). Position of time slices are indicated by dashed yellow lines. (c) Lower amplitude time slice through the platform, illustrating a possible initiation as two aligned platforms. (d) Upper amplitude time slice through the same platform, showing a single pattern of concentric rings. (e) Interpretive sketch diagram of platform growth. Colors of interpreted geomorphic elements are as noted in Figure 8(f). Red triangles indicate the seismic sequences discussed in the text.

(2) UC-2 Platforms. The flanks of many UC-1 platforms (e.g., capped by the UC-2 surface) include reflectors that onlap at a position below the previous margin (Figure 13). In several instances, this onlapping package forms a nearly flat-topped, locally offlapping succession (Figure 13(a)) that extends up to 1 km away from UC-1 breaks in slope. This succession is capped by a reflector (a peak) that can be carried away from the UC-1 platform margins and towards the intervening lows (surface UC-2a of Figures 13(a) and 13(c)). At several locations, the interval between UC-2 and UC-2a thickens and forms a convex-up mounded feature with an internal reflector (Figures 13(a)–13(c)). Above these isochron thicks and atop some other subtle highs between UC-1 platforms (Figure 13(b)), a central nucleus of horizontal, parallel, low-amplitude reflectors pass laterally into inclined reflectors that downlap onto UC-2a. In time slices, some of these features are oblong, with elongation towards the northwest (Figure 13(d)). Similarly, reflectors above UC-2a prograde

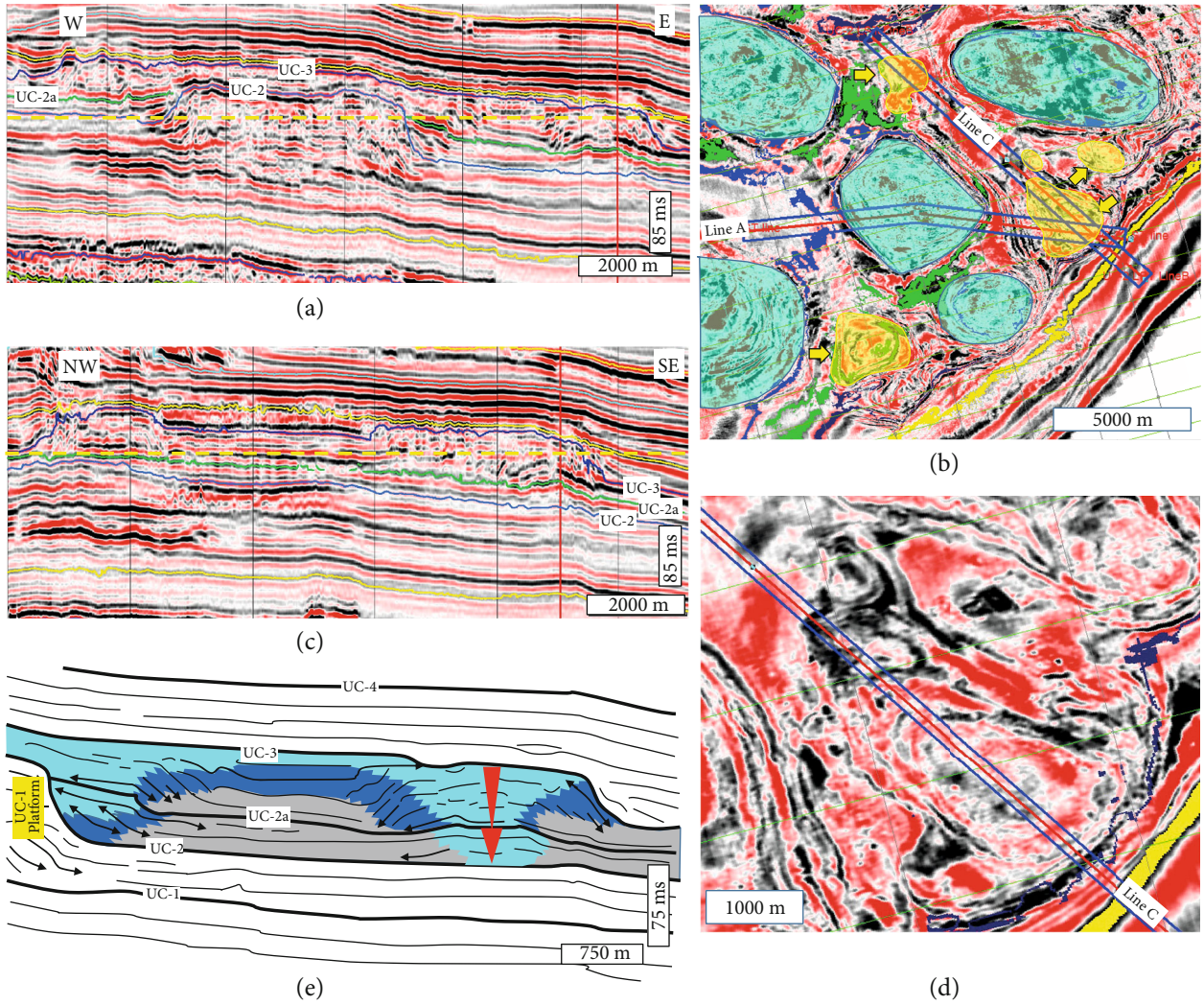

FIGURE 13: Seismic character of an illustrative UC-1 platform that continued and expanded into UC-2, Carbonate Platform Phase 4. (a) Seismic line through the platform. Position of time slice (b) is indicated by dashed yellow line. Note that horizon UC-2a onlaps the UC-2 surface (e.g., top of the UC-1 platform). (b) Amplitude time slice. Blue-colored areas represent UC-1 platforms, and yellow shades and yellow arrows highlight platforms of the basal part of UC-2 that initiated in interplatform lows. (c) Seismic line through two small UC-2 platforms, from a line through an interplatform low of UC-1 platforms. Position of time slice is indicated by dashed yellow line. (d) Zoom of amplitude time slice in part (b), showing the elongated growth to the northwest. (e) Interpretive sketch diagram of UC-2 platform growth for the right half of seismic line in part (a). Colors of interpreted geomorphic elements are as noted in Figure 8(f). See text for discussion.

from the flanks of UC-1 platforms and include offlapping reflectors that also downlap UC-2a (Figure 13(e)). Ultimately, the previous lows between platforms are filled by inclined, offlapping reflectors and overlying horizontal, parallel reflectors (cf. Figure 10(d)). Some areas include toplap that defines the UC-3 surface.

(a) Interpretation. As discussed above, at the scale of composite seismic units, the UC-2 platforms are interpreted to represent reinitiation, expansion, and amalgamation of the UC-1 platforms—essentially forming a continuation of those bodies. This gross trend is evident from the map view patterns of the UC-2 and UC-3 surfaces (Figures 7(a) and 7(b)) and in profiles of numerous platforms (Figures 10(a) and 10(d)). Nonetheless, the general pattern appears to be enhanced by the initiation of small isolated platforms in downdip lows between platforms (e.g., Figures 13(b), 13(d), and 13(e)). This initiation, which occurs low on the shelf, appears to have been facilitated by a relative fall in sea level, as evidenced by the onlap of terrace-like deposits (cf. [34]) below the margins of UC-2 platforms. These onlapping deposits are coincident with thickening below these downdip platforms. These platforms, as well as those that initiated on subtle highs in the basin, aggrade and ultimately prograde, merging with the platforms that reinitiated on the tops of UC-2 platforms once they were reinundated and transported excess sediment off the platforms.

(3) UC-3 Platforms. Parts of two large platforms are well imaged in the volume (Figures 14 and 15). One platform is

underlain by a subtle, east-west elongate isochron thick (between UC-3fs and S1 in Figure 14(a)). This thick is overlain by a progressively backstepping succession, culminating in a smaller mounded geometry of ~9.5 × 2.5 km (Figure 14(b), green polygon). A subsequent succession includes ubiquitous inclined oblique toplapping and downlapping reflectors that dip away from the highs of the S2 surface and are capped with the S3 surface. The S3 surface is in turn onlapped but then is flanked by a succession of offlapping reflectors that collectively mark progradation from the thick S3 (dashed blue line of Figure 14(b)). Progradation occurred to the north and to the south, but was greatest, up to 4 km, in a west-facing reentrant (Figure 14(b)). This platform is capped by the UC-4 surface, marked by onlap of strata below the previous shelf break (Figure 14(c)). This platform covered almost 200 km^2 within the survey area and included ~50 ms (85 m) of depositional relief.

A second platform includes a broadly analogous pattern of aggradation followed by progradation (Figure 15(a)), but with some marked distinctions. This appendage of a larger platform (Figure 7, upper slice) is oriented E/NE to W/SW and includes a subtle thick on the H1 surface; this thick occurs southeast of, but follows the trend of, a previous (UC-3) platform margin (Figure 15(a)). Above this thick, a succession of dominantly parallel, low to moderate amplitude reflectors is 40-60 ms (68-102 m) thick and capped by surface H2 (Figure 15(a)). This surface is marked by numerous irregular depressions up to 28 ms (48 m) deep (Figures 15(a) and 15(b)). These depressions extend up to several km in length parallel to the margin, or at least elongate in that direction and are most common on the northwestern part of the platform (Figure 15(b)). To the north and east, the H2 surface is marked by onlap of reflectors, features which are overlain in turn by a series of north- and east-dipping, shingled to oblique reflectors that mark up to 4.25 km of platform expansion (from dashed dark blue to light blue, Figure 15(c)). These dipping reflectors pass updip into low- to moderate-amplitude parallel reflectors on the previous highs and downlap or pass laterally into moderate- to high-amplitude parallel reflectors downdip (Figure 15(a)). The UC-4 surface overlies this succession and in turn is onlapped by strata below the previous shelf break, especially to the north of the platform (left and right sides of Figure 15(a)).

(a) Interpretation. These two features (Figures 14 and 15) both are interpreted to represent two UC-3 isolated carbonate platforms, but geomorphic and stratigraphic patterns are distinct between these platforms in several ways. First, the early stacking patterns are distinct (backstepping vs aggradational). Second, late-stage progradation was more pronounced to the south and west in one platform (Figure 14), to the north in the other (Figure 15). Finally, the second platform includes what appears to be pronounced karst (Figures 15(a) and 15(b)) at the turnaround from aggradation to progradation.

At a larger scale, they include several marked deviations from the trends of the older platforms in several ways. First, whereas UC-1 and UC-2 platforms nucleated as clusters of smaller circular to ovoid platforms, the oldest stages of UC-3 platforms appear as east/northeast elongated, but irregular, mounds. Second, whereas the UC-2 platforms generally represent expansion of UC-1 platforms, the spatial patterns of UC-3 platforms are quite distinct from those of UC-2 platforms (Figure 7). Third, in terms of growth, these platforms include early aggradational stages of largely vertical growth (Figures 15(a) and 15(c)) to aggradational to slight backstepping (Figures 14(a) and 14(b)), followed by marked progradation (Figures 14(c) and 15(d)) rather than centrifugal expansion and amalgamation with other nearby platforms more common in UC-1 platforms (Figures 10(c) and 11(b)).

(4) UC-4 Platforms. Two small isolated platforms are present in the lows between UC-3 platforms on top of the UC-4 surface (Figures 16(a) and 16(b)). The first platform includes an initial phase of parallel horizontal high-amplitude reflectors (surfaces 01 and 02 in Figure 16(c)) that define an E-W elongate body. Map view patterns in amplitude and similarity (Figure 16(d)) include roughly concentric, oval rings, extending to the west, that document a platform that grew to 6 km × 1.25 km in size. This thick is in turn surrounded by a series of inclined shingled to oblique reflectors capped by surface O3, with a broader belt of clinoforms to the west (Figure 16(e)). The north margin of this 10 km × 6 km platform merges with a set of inclined reflectors prograding from the large elongate platform to the north that downlap onto UC-4.

A second example formed in the reentrant of the southern UC-3 platform. This platform is circular rather than elongated and includes two high-amplitude parallel reflectors. It is surrounded and engulfed by NW- to NE-dipping clinoforms that represent expansion from UC-3 platform to the west and south (Figures 16(g) and 16(h)).

(a) Interpretation. Because they nucleate and grow from paleotopographic lows between UC-3 platforms (Figure 16(a)), these two features are interpreted to represent isolated platforms initiated following a relative fall in sea level. Relief from the tops of platforms to the basin floor of ~50 ms suggests a relative fall of as much as 85 m, to bring the previous deeper-water, intraplatform seaways to shallow-water setting. Although they both include an aggradational phase (capped by surface O2), the southern platform is more circular (Figures 16(g) and 16(h)), and the northern platform is elongated and includes offlapping patterns suggesting marked growth from east to west (Figure 16(f)). This centrifugal, but east-west elongated, growth (below surface O3) ultimately was over-run and subsumed by southward-prograding clinoforms from the reinundated northern platform. In contrast, the southern platform appears to have been covered by east- and north-prograding clinoforms from the reinitiated southern platform before it could expand (Figure 16(h)). The differences in shape and growth are interpreted to reflect a current-influenced setting of the northern platform, which drove asymmetric growth. In contrast, the more protected position for the southern platform favored more radial growth.

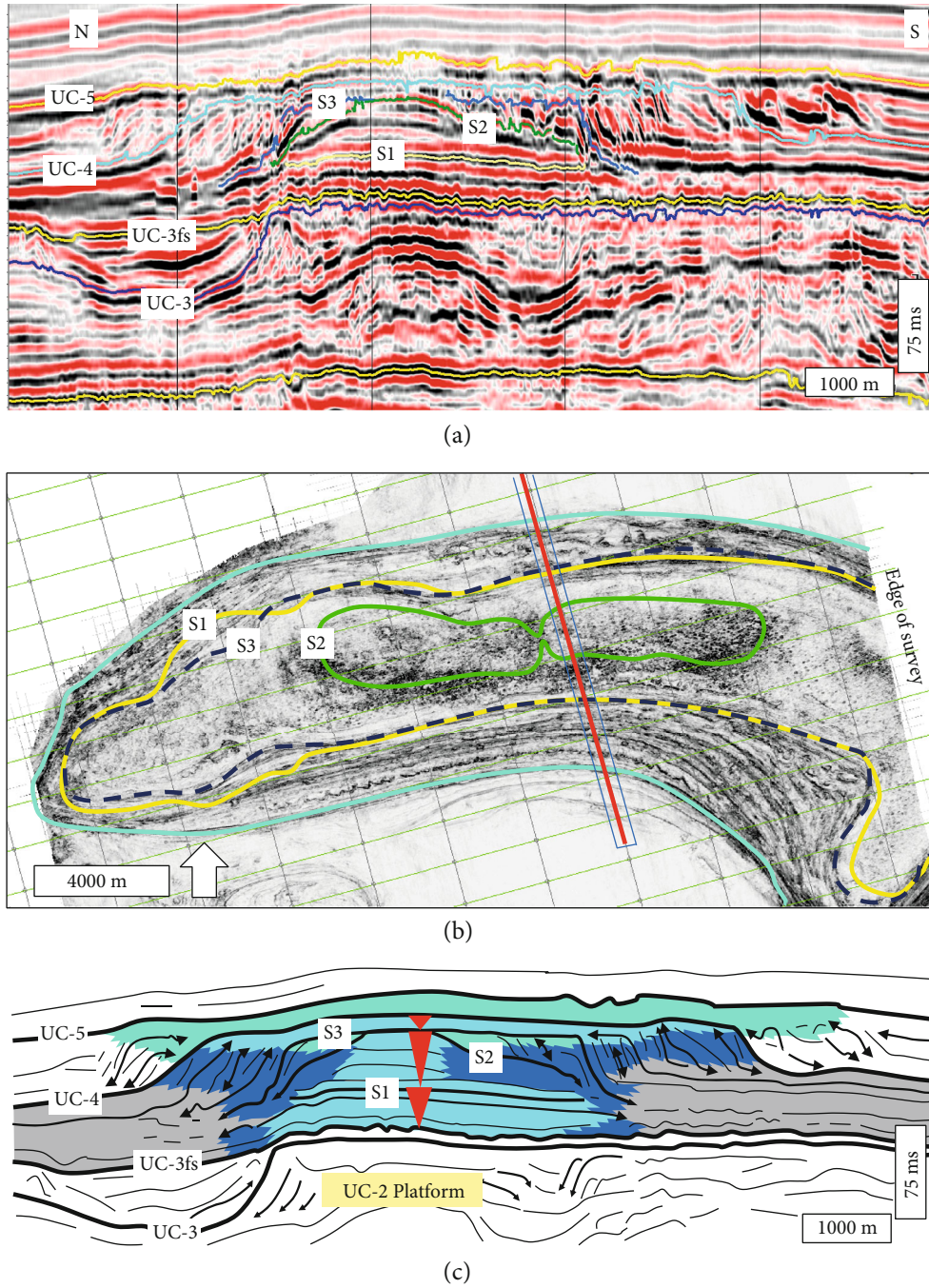

FIGURE 14: Seismic character of northern UC-3 platform (cf. Figure 7), Carbonate Platform Phase 4. (a) Seismic line through the platform, illustrating several internal surfaces (S1-S3). (b) Map of similarity, surface UC-4 (e.g., top of UC-3 platform). Polygons describe the position of the shelf break through time, from S1 to S2 to S3; light blue notes terminal margin. (c) Interpretive sketch diagram of platform growth. Colors of interpreted geomorphic elements are as noted in Figure 8(f). See text for discussion.

2.7. Platform Sizes. The results reveal a range of sizes and geometries of isolated carbonate platforms in this Miocene succession (Figures 17(a)–17(f)). Considering all platforms, sizes range from <400 m to >25 km across and reach areas in excess of 200 km^2, and they include synoptic relief of up to 200 m. Several collective trends are evident.

First, a plot of area versus relief (Figure 17(g)) indicates that platforms generally increase in size with time. The oldest succession, sequence set LC-0, includes abundant small, thin platforms, whereas the younger successions, the UC platforms, are larger and taller, but less numerous.

Second, the data indicate a general positive correlation between area and relief (Figure 17(g)). That is, larger platforms include greater relief, representing a collective log-linear trend.

Third, a plot of platform area versus exceedance probability (Figure 17(b)) illustrates that data form a linear, power-law like trend ($R^2 = 0.97$). The largest platforms, at

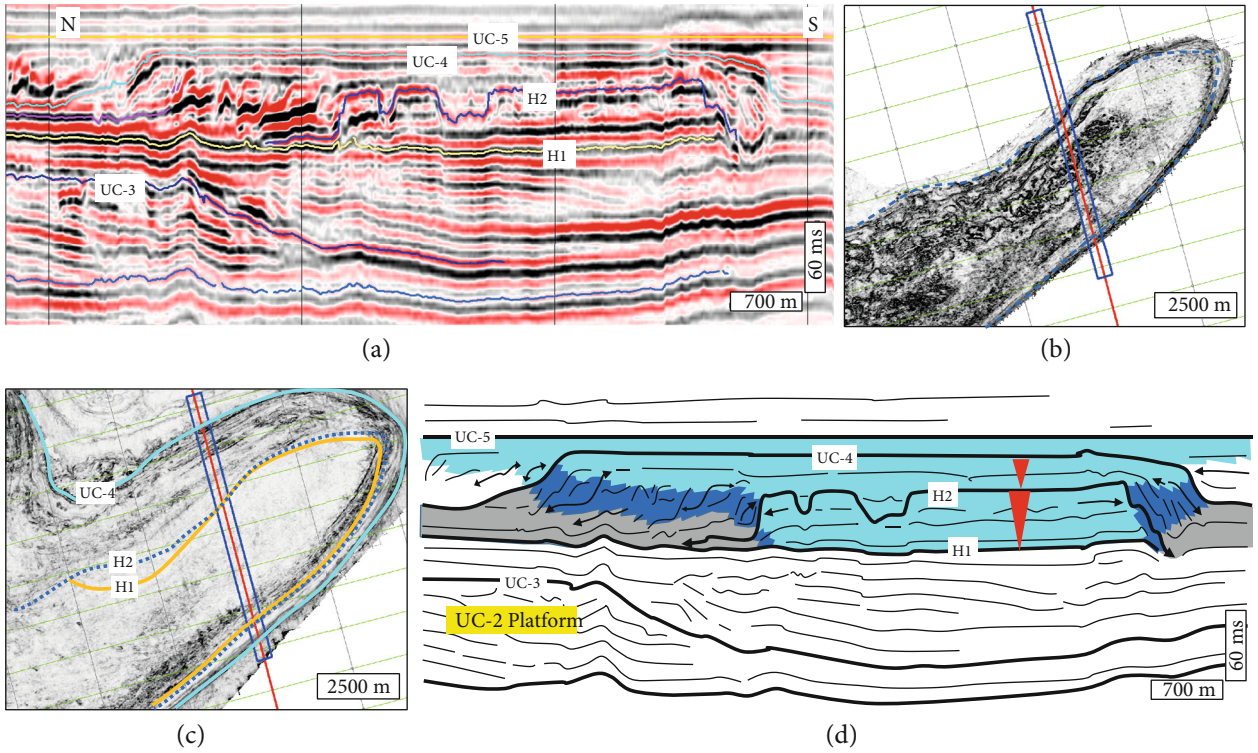

Figure 15: Seismic character of southern UC-3 platform (cf. Figure 7), Carbonate Platform Phase 4. (a) Seismic line through the platform; several internal horizons are noted (H1, H2). (b) Map of similarity, surface H2, illustrating the irregular pitted appearance of the northwest-facing part of the platform (cf. part (a)). (c) Map of similarity, surface UC-4, top of UC-3 platform. Polygons note the position of the shelf break for horizons H1, H2, and UC-4 is noted. (d) Interpretive sketch diagram of platform growth. Colors of interpreted environments are as noted in Figure 8(f). See text for discussion.

the right side of the plot, fall under the trend line; they are smaller than predicted. This artifact is not surprising, as each of these platforms marked by hollow circles (Figure 17(h)) extend beyond the survey area and thus are larger than the measurements indicate.

At a larger scale, these platforms are smaller than those evident in other systems. For example, the comparison of area of these Miocene platforms with mid to late Miocene platforms of Central Luconia, Malaysia [35], and modern atolls [36] reveals that these Northwest Shelf examples are smaller (Figure 17(i)). These Northwest Shelf platforms have a modal area of 0.08 km^2; Central Luconia Miocene platforms have a mode of 8 km^2, and modern atolls have a modal extent of 316 km^2.

3. Discussion

3.1. Impact of Eustatic and Global Oceanographic Processes. The Miocene was characterized by dynamic changes in oceanographic processes [7], atmospheric dynamics [12, 19], and biotic evolution [37], and each of these has the potential to impact the Miocene platforms of the Browse Basin. Aside from the global scale influences, a variety of processes at regional (e.g., Southeast Asia or Northwest Shelf) to local (Browse Basin or smaller) scale may impact these platforms. Comparison among the ages of strata and marked unconformities, faunal associations, and stratal geometries in this system and other Miocene carbonate platform systems across the globe reveals important similarities, as well as some marked contrasts, among areas (Figures 18, 19(a), and 20).

3.2. Central Luconia Province, Malaysia. The Central Luconia Province forms part of the broad shelf offshore of Borneo, Malaysia. During the early Miocene, this area included active tectonism and a marked influx of siliciclastics. By the middle Miocene, a relative rise in sea level and decrease in the rate of siliciclastic sediment input created conditions that favored the development of over 200 carbonate buildups across the region [38–40].

Above basal siliciclastics, many of these platforms include a lower, Langhian to late Serravaillian phase of broad low-relief platforms, termed the "megabank" stage by Vahrenkamp [40] and Koša [41]. These older buildups, described as the basal part of many of the isolated carbonate platforms ([40, 42], in press; [43, 44]), form part of what is locally noted as "Cycle IV" carbonates [45]. These broad, low-relief buildups commonly are overlain by a marked backstep [38] and by platform strata that either progressively backstep with intermittent subaerial exposure [11] (Figure 19(b)), aggrade vertically [42, 46], or alternatively backstep and prograde [44]. In almost all instances, however, these "Cycle V" platforms (late Serravaillian to Tortonian) are less expansive than the underlying Cycle IV platform (Figure 19(b)). The

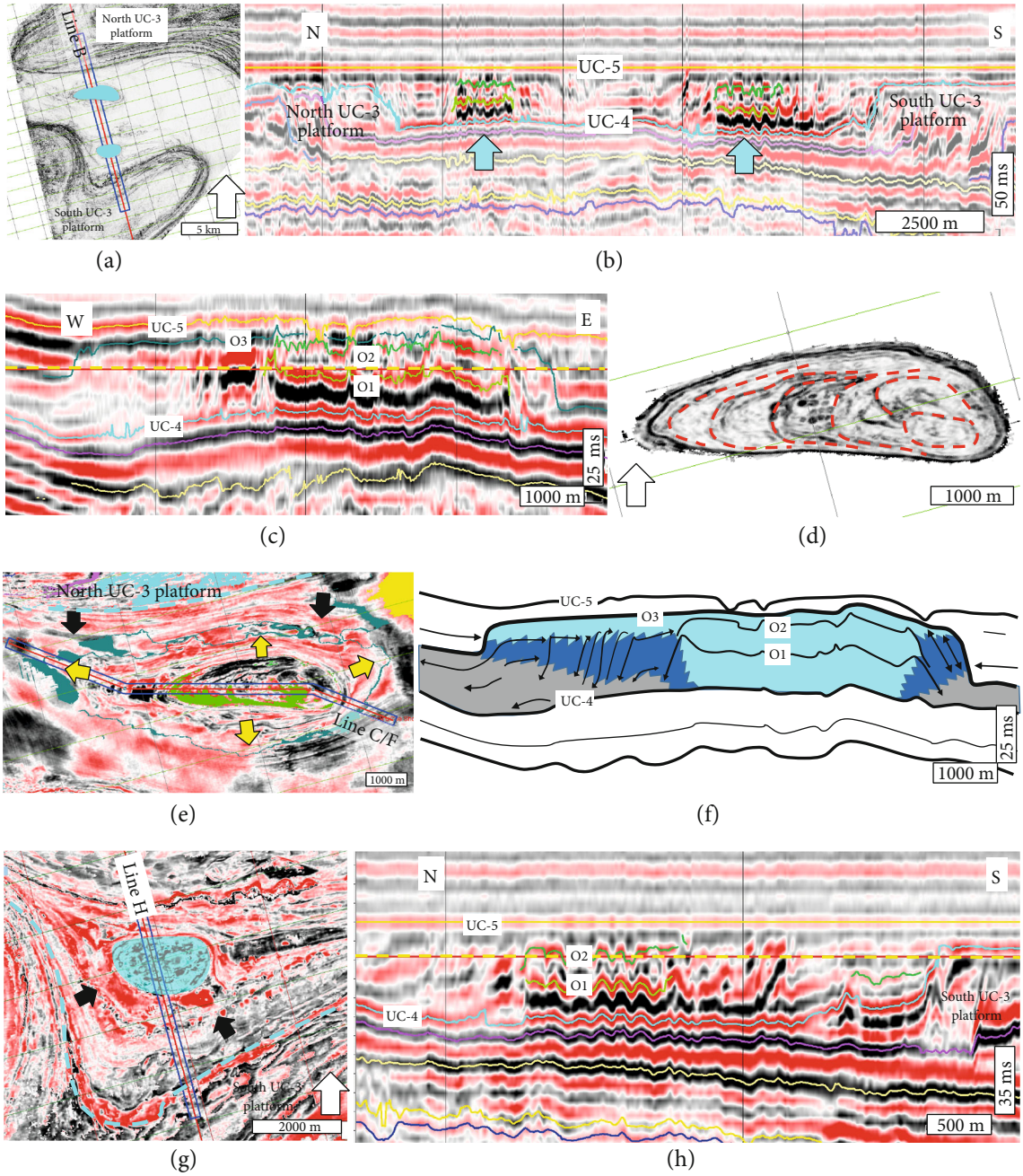

FIGURE 16: Seismic character of UC-4 platforms, Carbonate Platform Phase 4. (a) Similarity map, surface UC-4, noting the location of the line in part (b). The two platforms of UC-4 are shaded blue. (b) Seismic line flattened on UC-5 that crosses the two platforms. Platforms, emphasized by the teal blue arrows, nucleated and expanded in the interplatform low between the northern and southern UC-3 platforms. (c) Seismic line through the northern UC-4 platform, illustrating internal architecture. Position of time slice (part (e)) is indicated by dashed yellow line. Line location is illustrated in part (e). (d) Similarity on horizon O2, illustrating westward growth. (e) Amplitude time slice. Note the radial growth (yellow arrows), with the greatest expansion to the west. Ultimately, the rejuvenated platform to the north prograded over this smaller platform (black arrows). (f) Interpretive sketch diagram of platform growth. Colors of interpreted geomorphic elements are as noted in Figure 8(f). (g) Amplitude time slice. Position of time slice is indicated by dashed yellow line in part (h). (h) Flattened seismic line through the southern UC-4 platform, illustrating internal heterogeneity. Note that this platform is surrounded by north- and east-prograding clinoforms of sediment derived from the rejuvenated south platform. Line location is illustrated in part (g). See text for detailed discussion.

platforms are dominated throughout by a photozoan assemblage, including scleractinian corals, red algae, and foraminifera; lithologies range range from grainstone to floatstone to sudstone, and some framestone although wackestone and packstone with planktonic foraminifera define flooding and backstepping intervals (e.g., [43, 44, 47]). Many of these

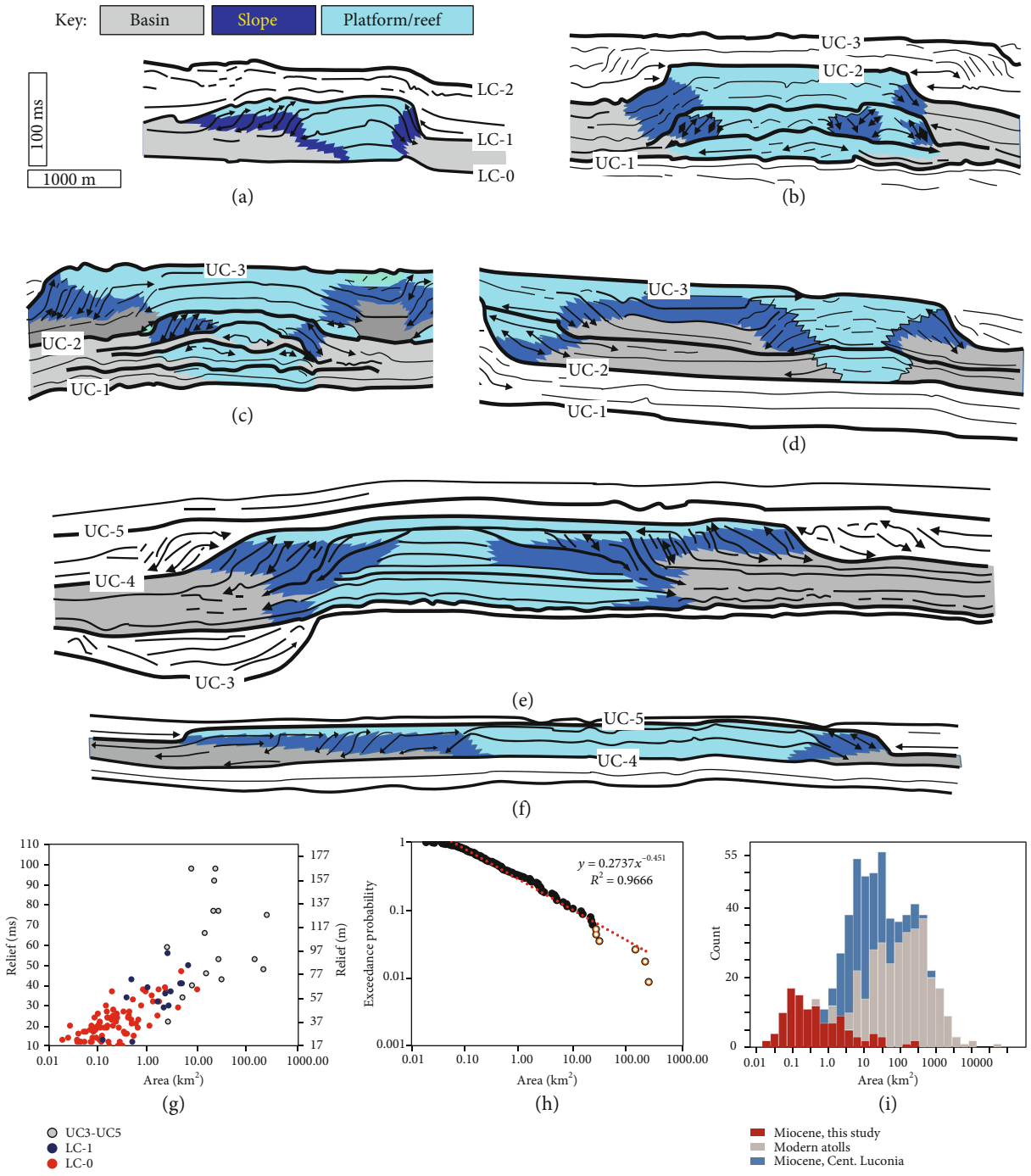

FIGURE 17: Size comparisons among platforms. (a–f) Plots of various platforms, all shown at the same scale. Note the wide range of sizes, stacking, and thicknesses. (g) Cross-plot of platform area (on a log scale) versus relief, subdivided by seismic stratigraphic unit. Note the general correlation and that CPP-4 includes generally larger and taller platforms. (h) Cross-plot of platform area versus exceedance probability (both on log scale). Platforms not completely within survey are noted with open circles; they tend to fall below the trend line (smaller than predicted). Note the general power-law correlation, broadly comparable to that of populations of patch reefs (e.g., [27]). (i) Size-frequency histograms for these middle to late Miocene platforms, middle to late Miocene platforms of Central Luconia (Malaysia) [35], and modern atolls [36]. Note the distinct populations; see text for discussion.

platforms drowned in the late Miocene (Figure 19(b)) [40, 44, 47], although some of those far offshore continue until today (Kosa et al., 2016). Several of the terminated platforms are onlapped and overlain by carbonate drift deposits [11] (Figure 18).

These general patterns recently have been interpreted to reflect carbonate platform response to the dynamics of Miocene global processes. Specifically, Mathew et al. [11] posit that tectonics and eustasy drove platform growth patterns (Figure 18). They suggested that Langhian initiation of

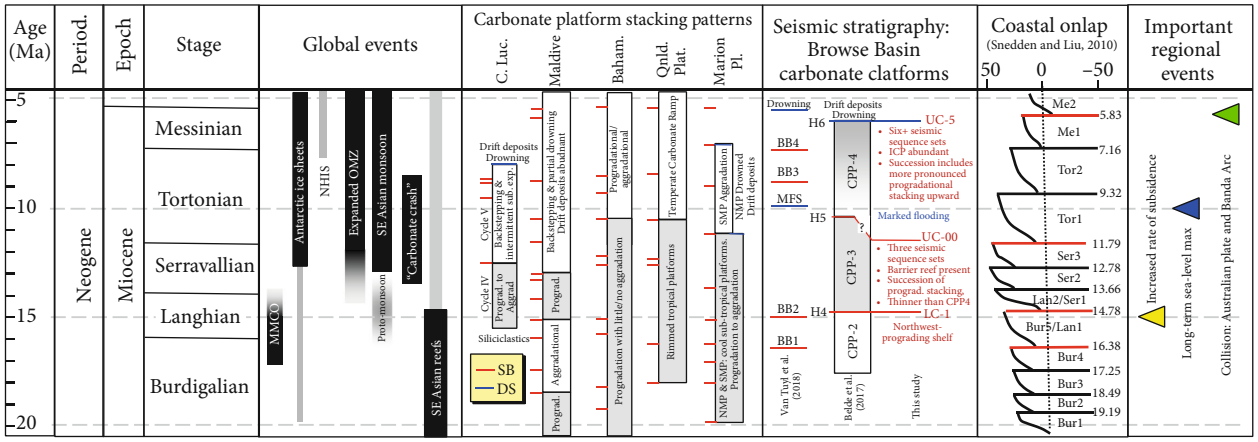

FIGURE 18: Chart summarizing Miocene oceanographic, stratigraphic, tectonic, and eustatic trends and relation to Browse Basin platform seismic stratigraphic patterns documented herein. Columns include the following: (i) global events, summarized from Mathew et al. [11] and references therein. (ii) Stacking patterns of well-documented Miocene carbonate platforms. Red lines represent sequence boundaries (dates in Figure 20); blue lines are drowning surfaces; subcolumns describe sequence stacking patterns (cf. Figure 19). Those columns shaded grey include more pronounced progradational stacking patterns. C. Luc. = Central Luconia, summarized from Mathew et al. [11]. Maldive = Maldives, from Betzler et al. [7]. Baham. = Bahamas, from Eberli and Ginsburg [34, 54] and Eberli et al. [55]. Qlnd. Plat. = Queensland Plateau, from Betzler et al. [62]. Marion Plat. = Marion Plateau, from Eberli et al. [74]. Note that several of these studies have proposed global correlations based on similar ages and numbers of sequence bounding surfaces. (iii) Seismic stratigraphy and major surfaces of the study area, defined by Van Tuyl et al. [28], Belde et al. [25], and this study. (iv) Coastal onlap, from Snedden and Liu [78], with eustatic falls that they characterized as pronounced marked by red lines. (v) Other important events that potentially affected the area. See text for discussion.

platform FX at 15.5 Ma and growth of the laterally extensive Cycle IV carbonates were favored by a long-term eustatic peak in the middle Miocene (Mathew et al. 2020). Subsequent late Serravallian to middle Tortonian platforms in Central Luconia transition from progradational-aggradational to backstepping at SB1, dated at 12.5 Ma [11]. This change was interpreted [11] to be shaped by the slow eustatic turnaround, a strengthening SE Asia Monsoon, and a decrease in carbonate production rates (broadly related to the "Carbonate Crash"). Monsoon intensification and enhanced currents after 9.5 Ma may have led to backstepping platforms, with periodic subaerial exposure, including the sequence boundaries dated at 9.5, 8.8, 8.6, and 8.0 Ma on platform FX [11] (Figure 19(b)).

3.3. Maldives. The Maldives are an equatorial chain of atolls in the Indian Ocean southwest of India (Figure 19(a)), with negligible siliciclastic influx throughout the Neogene. There, two parallel, north-south oriented rows of atolls encircle the Inner Sea, which can reach water depths of up to 500 m.

Representative seismic lines through the Neogene succession of the Maldives document a complex stratigraphy (Figure 19(c)). A thin succession of Paleogene neritic carbonates that nucleated on paleo-highs is overlain by a 2000+ m-thick succession of shallow water carbonates [48, 49]. Following the Oligocene succession, a pronounced drowning event flooded the platform, and the subsequent platforms were much narrower [7, 50]. Seismic-stratigraphic characterization of the overlying early to middle Miocene succession (Figure 19(c)) describes an early buildup stage that started with an east-dipping carbonate ramp that aggraded and gradually steepened as it started as aggradational but gradually changed to subtly progradational by 18.5 Ma. Between 18.5 Ma and 15 Ma, the platform shifted to largely aggradational, before changing to more progradational after 15 Ma (Figure 19(c)). This change from aggradation to progradation at 15 Ma is coincident with a change in carbonate factory, from the older successions of coralgal reefs to larger benthic foraminifera-calcareous algae dominated strata in younger strata [51], although coral-coralline algal boundstone occurs at the shelf margin in the progradational units [52]. Following a period of subaerial exposure [52], at 12.9-13 Ma, carbonate systems across the archipelago underwent an abrupt shift to drift deposits (Figure 19(c), noted as Drift Sequences, or "DS"), rather than resuming the expanses of shallow-water carbonate deposition (e.g., [51]). Nonetheless, the double row of atolls represents neritic carbonate deposition that continues today.

Many of these patterns have been interpreted to reflect eustatic controls on the early to middle Miocene carbonate systems, followed by a shift to current-controlled sedimentation from the middle Miocene to the Pleistocene [7, 50–52] (Figure 18). The early, aggrading ramp corresponds to eustatic rise and high. Leading up to and during the Middle Miocene Climatic Optimum, the platform systems were linked closely to eustatic change—aggrading stacking patterns caused by eustatic highs, and progradational seismic geometries reflected eustatic falls [7]. The change from aggradation to progradation and shift in faunal association at 15 Ma also occurred during the Middle Miocene Climatic Optimum. The subsequent abrupt shift to drift deposits accompanied a decoupling of sedimentary and stratigraphic patterns from eustatic change after 13 Ma [51, 52]. Instead, drift deposits have been interpreted to reflect intensification

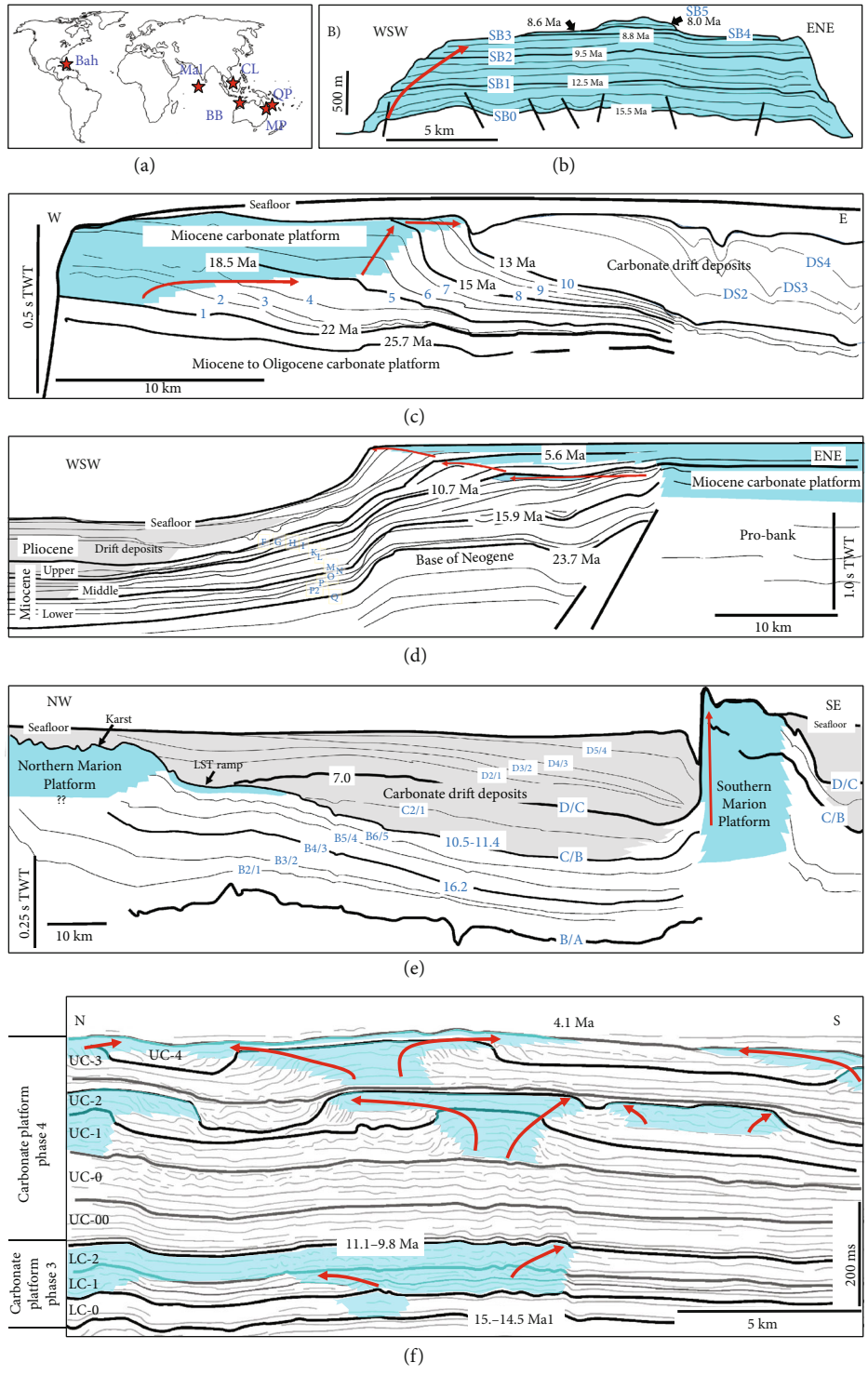

Figure 19: Comparison of sketch summaries of seismic sequence stacking patterns of well-studied Miocene carbonate successions. (a) Locations of study areas. Bah = Bahamas; Mal = Maldives; CL = Central Luconia; QP = Queensland Plateau; MP = Marion Plateau; BB = Browse Basin. (b–f) Stacking patterns, identification and ages of sequence boundaries, and facies patterns. Each plot has a different scale and vertical exaggeration. Note that the *y*-axis of part (b) is in depth and the others are in time. Major sequence boundary surfaces, as identified by the original authors, are marked in bold with their ages explicitly noted. The ages of sequence boundaries (blue font) are listed in Figure 20. Blue represents interpreted distribution of shallow water, platform-top strata. Red arrows represent general trend of shelf-margin trajectory in each plot. (b) Platform FX, Central Luconia, offshore Malaysia. Modified from Figure 3(c) of Mathew et al. [11]. (c) Maldives Inner Sea line. Modified from Figure 2 of Betzler et al. [7]. (d) Bahamas, line 106 merged with Western Line. Modified from Figure 9 of Anselmetti et al. [58]. (e) Marion Plateau, seismic line MAR20. Modified from Figure 9 of Eberli et al. [74]. (f) Torosa survey, Browse Basin, Northwest Shelf, Australia. Modified from Figure 2 of this study.

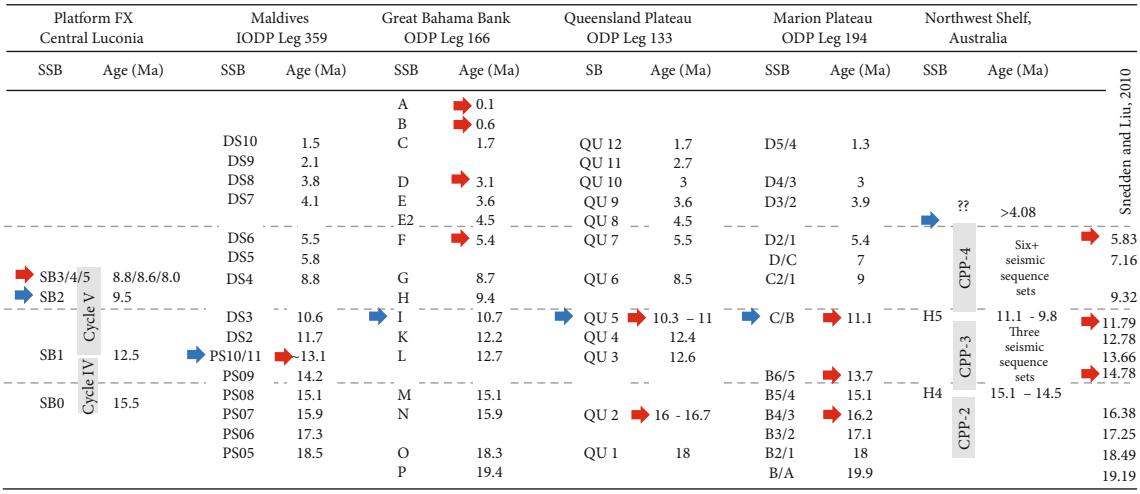

FIGURE 20: Summary of ages of sequence boundaries in well-constrained, Miocene and younger carbonate successions. Data include Central Luconia [11], Maldives [7, 52], Bahamas [55], Marion Plateau [74], and Queensland Plateau ([62], Betzler et al. [76], Brachert et al. [77]) and Northwest Shelf, Australia ([25], sequence information from this study). The sequence nomenclature refers to those surfaces documented on Figure 19. The ages of sequence boundaries from Snedden and Liu [78] are illustrated for reference as well. Dashed grey lines are intended to aid in visualizing comparisons among areas, not necessarily correlations, and represent roughly every 5 Ma. The red arrows note especially prominent subaerial exposure surfaces noted by the authors, whereas blue arrows represent the onset of marked deposits of carbonate drifts. Note that the bounding surface at the top of CPP-3/base of CPP-4 appears roughly coincident with major changes in many other areas, but the base CPP-3 horizon and top CPP-4 horizon do not appear to have simultaneous major changes in other areas. Similarly, the number of sequences and sequence sets do not appear to correlate among areas.

of the monsoon, which led to stronger currents and upwelling and drowning of some of the platforms [7, 8].

3.4. Bahamas. The Great Bahama Bank represents a very large isolated carbonate platform whose history of shallow-water carbonate accumulation began in the Cretaceous [53]. The succession as a whole documents warm, tropical to subtropical photozoan carbonates deposited on a passive margin.

On lines from west of Andros Island, seismic data document platform dynamics through the Neogene across the present-day bank top to the margin and into the Straits of Florida (Figure 19(d)). Seismic stratigraphic interpretations [34, 54] illustrate the presence of several proto-banks, separated by channels, which gradually infilled. Seismic stratigraphic interpretations document a stage [34, 54] of late Oligocene to middle Miocene westward progradation from the Andros bank that filled one of the larger seaways, the Straits of Andros, and expanded the bank to the west, areas which had been more aggradational prior to then (Figure 19(d)). Subsequent platform growth from the late Miocene to recent is characterized by aggradation and progradation west of the then-expanded Andros Bank (Figure 19(d)) [34, 55–57]. This general pattern of aggradation to aggradation-progradation consists of higher-frequency sequences of sigmoidal to sigmoidal-oblique clinoforms roughly 500 to 600 m tall, many of which include strata that onlap below the previous shelf margin (Figure 19(d)) [34, 58].

These patterns were interpreted [34, 55, 58] to reflect the influences of eustasy, but with growth patterns facilitated and influenced by currents. The two-part subdivision (middle Miocene and older versus post-middle Miocene) appears to correspond to second-order eustatic cycles described by Haq et al. [59]. In their conceptual model [34], the older, pre-middle Miocene seismic sequences, which are more progradational, reflect periods when the platform top is hardly flooded and most sediment is transported offbank. In contrast, the younger progradational to aggradational sequences were interpreted to have been deposited during long-term rises in sea level and the more aggradational components favored by greater sediment production on the broad, inundated platform top. Individual seismic sequences were matched to distinct third-order cycles of eustatic change of the Haq et al. [59] curve [34, 55, 58].

In addition to sea level, currents influenced the geometries that are evident in seismic, in both slope and basinal areas [34, 60]. The overall asymmetric, westward slope progradation was interpreted to reflect the greater energy on the eastern, windward margin, which drove westward transport of bank-derived sediment and favored platform progradation of 25 km in that direction. Aside from shallow bank-top, wind-driven currents, carbonate drift deposits generated by deep-water currents are dominant in basinal locations within one middle Miocene sequence and from the late Miocene to Recent. These processes, enhanced starting in the latter part of the middle Miocene, reflect stronger ocean currents, such as the Florida Current [58].

3.5. Queensland Plateau. Located in the low-latitude western Pacific, the Queensland Plateau lies offshore of northeastern Australia. This plateau represents a partly drowned isolated carbonate platform far from a terrestrial landmass on a passive margin [61]. As such, it has been, and remains, free from any marked influence of siliciclastics. Accumulation of Cenozoic carbonates started in the middle Eocene, with bryozoan,

larger benthic foraminiferal sediment, reflective of temperate water with some warmer incursions through the late Oligocene [61–63].

Overlying middle Eocene strata of this area are upper Oligocene carbonates, reflecting a major unconformity. The carbonates include bryozoan-rich packstones. Above another unconformity, lower Miocene strata consist of wackestone to rudstone with larger benthic foraminifera, red algae, *Halimeda*, and corals, with facies reflecting deposition in reefs, shallow-water lagoons, and periplatform settings [63]. These deposits have been interpreted to reflect initiation of a subtropical to tropical chlorozoan-association rimmed platform that grew and thrived through the early and middle Miocene ([61, 62], 2000), with no evidence of subaerial exposure [63]. These faunal patterns are consistent with paleogeographic estimates, which place the region between 24°S and 29°S during this time, with continued northward movement.

At 10.7 Ma (earliest late Miocene), strata reflect a marked change in faunal associations and stratal geometries ([63, 64], 2000). Deposits include an increase in pelagic deposition and an increase in periplatform deposits such as planktonic foraminifer and calcareous nannoplankton oozes [62]. These strata reflect warm- to temperate-water bryomol-association carbonates that formed a carbonate ramp from the late Miocene into the early Pliocene. Unlike the early and middle Miocene section, these units include no tropical photozoan reefs, although local bryozoan-mollusk buildups are present. Onlap of upper Miocene strata onto middle Miocene buildups suggests progressive flooding during this interval [62, 64].

At a larger scale, these patterns have been interpreted in the context of tectonic, eustatic, and oceanographic change ([63, 64], 2000). Early Miocene initiation of tropical to subtropical, photozoan sediment may reflect warming favored by northward equatorward drift of Australia. This warming was coupled with paleocirculation changes marked the onset of southward flow of warm waters from the equatorial Pacific into the area [65, 66]; both tectonic drift and paleoceanographic change favored the warm-water flora and fauna [63]. Enhanced subsidence favored continued carbonate deposition through the middle Miocene. Because Australia continued to migrate north towards the equator during this time, the abrupt change at 10.7 Ma to nontropical cooler-water carbonates was not due to tectonic drift out of the tropics [63, 66]. Instead, this faunal change has been interpreted to reflect a decrease in the rate of carbonate production on platform top and slopes, in turn related to the expansion of cooler water of less than 20°C (Betzler et al. [76]). This cooling was linked to global climate deterioration after the Middle Miocene Climatic Optimum and transition to the "Carbonate Crash" [67–69], ocean reorganization that weakened the South Equatorial Current, and a subsidence pulse ([63, 66]; Betzler et al. [76]).

3.6. Marion Plateau. The Marion Plateau is a modern shelf appendage off the east coast of Australia. It overlies a Neogene passive margin succession that includes both carbonates and siliciclastics. The oldest sediment drilled above basement is Oligocene, and in the Miocene interval, siliciclastics are most abundant in distal slope and basinal settings, where they can form up to 53% of the sediment [70]. The Marion platforms examined by ODP Leg 194 represent parts of two Miocene platforms (Southern Marion Platform and Northern Marion Platform) and associated slope and basinal strata (Figure 19(e)).

The Northern Marion Plateau includes more than 300 m of prograding clinoforms of fine-grained packstone, interpreted to represent the distal slope of another platform [70]. These strata are capped with a surface dated at 16 Ma and then overlain by transparent to chaotic seismic package of shallow-water bioclastic limestone with dolostone, representing aggradational platform deposits (Figure 19(e)). This facies offset, of shallow platform strata overlying distal slope deposits, was interpreted to reflect a major relative fall in sea level at 16 Ma ([70]; Eberli et al., 2004). A second relative fall in the late middle Miocene (13.4-11.4 Ma) subaerially exposed and karstified the aggrading platform (Horizon C/B of Figure 19(e)). An upper Miocene succession drilled off the flank of the platform included bryozoan-dominated packstone and floatstone, interpreted to represent "lowstand ramp" deposits [70, 71]. The shallow-water Northern Marion Platform never fully recovered from the subaerial exposure, however, and it is capped by a thin cemented layer of phosphatic foraminiferal wackestone to packstone dated at 9.6 Ma and then hemipelagic deposits dated at 5.5 Ma [72], indicating a prolonged omission surface.

The Southern Marion Platform (SMP) indicates a distinct history (Figure 19(e)). Overlying the latest Oligocene siliciclastic phosphatic sand, the initial platform succession consists of aggrading rhodalgal deposits, passing downdip to benthic foraminiferal-skeletal grainstone and rhodalgal-foraminiferal floatstone [70]. By early middle Miocene (16.4 Ma), the platform was dominated by coralline algae and miliolid foraminifera and developed marginal reefs. The middle Miocene system became markedly asymmetric, including a steep, escarpment-like rimmed western (upcurrent) margin and an eastern (downcurrent) margin of lower gradient clinoforms that were dominated by rhodalgal floatstone (Figure 19(e)) [70]. Contemporaneous drift sediment deposited between platforms largely includes clay-rich mudstone to wackestone rich in planktonic foraminifera (e.g., between surfaces C/B and D/C, Figure 19(e)). The platform drowned in the latest Miocene, although intermittent growth occurred locally through the early Pliocene [73]. Although no subaerial exposure is evident, the SMP was impacted markedly by diagenesis, including leaching, cementation, and dolomitization, and is seismically transparent, precluding confident correlation of surfaces through the platform [74].

These successions reflect eustatic and oceanographic change. During the early to middle Miocene, the platforms and associated strata include progradational to aggradational sequences that closely reflect eustatic change, as sequence boundaries have been correlated to the Queensland Plateau and the Bahamas [74] (Figure 18). In contrast, late middle Miocene and younger strata reflect both sea level change and coupled current action. Northward migration of Australia disrupted the equatorial currents and initiated the southward-flowing East Australia Current, which then

impacted the Marion Plateau (as it did the Queensland Plateau carbonates, above). This enhanced current started at 13.4 Ma but increased markedly at 11.4 Ma [75]. Sea-level changes modulated currents, as relative falls intensified currents between platforms and favored drift deposits. Although relative rises reflooded platforms, brisk currents on the platform tops prevented reinitiation of prolific production [74]. Currents swept across the top of the subtropical, heterozoan platforms, since their tops were at water depths of 30-40 m, and controlled the marked platform asymmetry [74] (e.g., Figure 19(e)). The different ages of drowning (top middle Miocene, 11.1 Ma, for the NMP, latest Miocene, 7 Ma, for SMP; Figure 19(e)) may reflect earlier and stronger current impact on the more proximal NMP [74].

3.7. Synthesis: The Influence of Global Processes on the Northwest Shelf. The ages of seismic sequences have been dated in many areas, and correlations among areas have been cited as evidence of eustatic change. Specifically, comparisons of the number and ages of sequences among areas suggest similarities (Figure 20), and therefore were interpreted to reflect a eustatic signal across areas (e.g., [34]; Betzler et al. [7, 11, 74, 76]), although each of these authors carefully describes the influence of complicating factors, such as tectonics and paleoceanographic change.

As this study offers no new absolute ages of Northwest Shelf sequence sets and component sequences, such a direct sequence-by-sequence correlation is not possible. Nonetheless, it is informative to compare the first-order seismic stratigraphic patterns within the established chronostratigraphic framework of the Northwest Shelf composite sequences [25] and to explore the implications with regards to global processes.

The first pronounced depositional shift considered herein occurs at the base of the succession at the CPP-2 to CPP-3 transition, within the mid-Langhian (~15 Ma) (Figure 19(f)). At this time, carbonate depositional systems shifted from a shelf prograding northwest towards the open ocean (strata of CPP-2) to isolated platforms that amalgamated into a barrier reef and platform system expanding into an intrashelf basin (CPP-3; Figures 1(c) and 2) ([25, 28], this study). The marked geomorphic shift may reflect the influence of several factors.

First, a mid-Langhian (15.1–14.5 Ma) relative fall of sea level could have terminated the carbonate systems of the CPP-2 shelf. The marked shift across this surface—a backstep from a seaward-prograding carbonate shelf to isolated platforms, followed by amalgamation and landward progradation of a "barrier reef" system—could be coincident with a eustatic fall (14.78 Ma, described as a major event by [78]) and subsequent rise. Yet, sequence stacking patterns here (progradation then a backstep) are nearly opposite those in the Maldives (a change from aggradation to purely progradation) (compare Figures 19(c) and 19(f)) Similarly, no major change is evident in sequence stacking patterns in the Bahamas around this time [34, 55, 58], and this transition clearly post-dates the 16 Ma fall documented in the Marion Plateau and the Queensland Plateau (Betzler et al. [74, 76]). Collectively, these discrepancies suggest that eustasy is not a sole control on this change at ~15 Ma.

Second, this change could reflect the gradual cooling that represented exit from the Middle Miocene Climatic Optimum and transition to the Carbonate Crash [68, 79]. Both of these factors could be expected to lower the carbonate saturation state, and this reduction also could have influenced the carbonate accumulation rate on the Northwest Shelf [29]. An interpretation of this change reflecting an event of global importance is inconsistent with the data, however. This shift, from CPP-2 to CPP-3, is roughly coincident with shift in sediment type in Central Luconia, which changed from siliciclastic- to carbonate-dominated systems within Cycle IV [38, 41], recently dated at 15.1 Ma [11] (Figure 20). Similarly, the Maldives platform shifted from more aggradational prior to 15 Ma to exclusively progradational, reflecting excess sediment production rather than a decline in production, until 13 Ma (Betzler et al. [76]). Thus, although stratal patterns in CPP-3 appear to reflect lower rates of carbonate production, a synchronous, global reduction in carbonate production seems an unlikely cause.

Finally, the rate of subsidence in the area, which increased from 60 m/Ma [80] to 125 m/Ma [25] after 15 Ma, may have caused a relative rise in sea level. Such a dynamic may have limited carbonate production across the shelf and focused it initially in more localized accumulations, such as isolated platforms (Figures 2, 4, 5, and 6). Ultimately, however, in the survey area, the carbonate production recovered. Localized platforms amalgamated during CPP-3, and the barrier reef system that was located seaward (NW) of the study area [25] prograded landward (SW) into and across the area, subsuming and enveloping the previously isolated platforms (Figures 1(c), 5, 6, and 9). A subsidence event could also have had regional variability as well (cf. [25]), perhaps even causing the apparent reversal of the trend of progradation (to the west during CPP-2, to the east during CPP-3).

A second pronounced event in the survey area occurs at the transition from CPP-3 to CPP-4 (horizon UC-00 of Figures 1 and 2), when the broad shelf was flooded and downlapped. The age of this change was approximated as Tortonian by Belde et al. [25]. Their age, based on Sr dates from strata that bound H5 (presented by [24]), includes dates of 11.1 Ma (below) and 9.8 Ma (above) that bracket this horizon with age uncertainties of ±1 Ma.

This horizon could thus correlate with (i) the major eustatic fall described by Snedden and Liu [78] at the Serravallian-Tortonian boundary, at 11.79 Ma, or (ii) the major events around 10.7 Ma (e.g., Betlzer et al. [74, 76]). Although a correlation with the 11.79 Ma fall would make this horizon older than suggested by Belde et al. [25], it does lie within the uncertainty of the data. At a larger scale, it would also be consistent with the prediction [78] of three sequences in the time interval that CPP-3 would have been deposited (e.g., between 15 Ma and 11.79 Ma, Figure 18). Similarly, the possible karst and incision (Figures 6(g) and 6(h)) are congruent with this interpretation.

Nonetheless, a conservative correlation might be more consistent with the dates suggested by Belde et al. [25]. That correlation would not have correlation in timing or number of sequences with Snedden and Liu [78], but would make

the CPP-2/CPP-3 transition coincident with the major subaerial exposure surface at 10.3-11 Ma in Queensland and 10.7-11.0 on the Marion Plateau [72, 74]. Likewise, it would correlate with the surface of marked middle to late Miocene change in seismic-sequence stacking patterns documented in the Bahamas, which shifted from largely progradational to combined aggradation and progradation (Figure 19(d)).

In this scenario, however, this eustatic fall would have impacted platforms differently. For example, patterns in Central Luconia [11] document continued backstepping after the 12.5 Ma sequence boundary until platform termination at 8.0 Ma (Figure 19(b)). Likewise, the Maldives platforms were characterized by progradation between 15 Ma and 13 Ma, after which there was an abrupt shift to drift sediment [7] (Figure 19(c)). The Maldives and Luconia regions were influenced directly by the SE Asian Monsoon during this interval; however, so this divergence may not be surprising [7].

Following deposition of the lower succession (CPP-3), shallow-water carbonate production appears to have ceased or slowed markedly, as suggested by low-angle downlaps and absence of well-developed platforms in the survey area. This apparent flooding is consistent with, and may have been favored by, factors including the following: (i) a relative rise in sea-level favored by rapid subsidence [25]; (ii) the long-term eustatic maxima during the Tortonian ([78]; note, however, that Haq et al., 1988 suggest a long-term high in the Langhian to early Serravallian, not the Tortonian); and (iii) continued suppressed carbonate production during the Carbonate Crash [68, 79]. Following flooding, however, CPP-4 indicates a progressive change from minor platforms to aggradational platforms to progradational platforms. These patterns are not inconsistent with several possible controls, including middle to late Tortonian long-term eustatic sea-level fall, rate of subsidence decrease, or waning impact of the Carbonate Crash (Figure 18).

The final event captured in the succession (top CPP-4, surface UC-5) appears to be preceded by a marked relative fall in sea level (surface UC-4). This fall is evidenced by platforms that initiated in paleo-seaway lows (Figure 16). This deposition, limited to lows, was followed by reinundation and expansion of the previous platforms (Figures 14–16). This marked fall could be 5.83 Ma eustatic fall [78], perhaps related to the pronounced 5.4 Ma fall recognized in the Bahamas (F, [55]), or the sequence boundaries recognized in the Maldives (D6, [7]), the Marion Plateau (D2/1, [74]), and the Queensland Plateau (QU7, Betzler et al. [76]).

Either way, this fall was followed by drowning. Belde et al. [25] suggested platform drowning was favored by enhanced currents. Alternatively, this drowning could reflect tectonic activity and an increased rate of subsidence related to collision of the Australian plate and the Banda Arc (Hall, 2012; [81]). Nonetheless, there is no evidence for fault control on platform margins or active syndepositional differential movement during this time (cf. [25, 28, 81]).

Although the timing of the first-order changes and the bounding surfaces of CPP-4 are consistent with those patterns expected if they were driven by global eustatic and chemical oceanographic processes, numerous seismic-stratigraphic details are not. For example, the number of sequence sets (six) in CPP-4 cannot be reconciled with Snedden and Liu [78], who suggest three sequences. Likewise, the Torosa data (i) contrast the Bahamas succession [34], which includes three sequences, units that are aggradational to progradational during this interval, and (ii) are distinct from patterns of the Queensland and Marion plateaus platforms. The Queensland Plateau was interpreted to include only two sequences (Betzler et al. [76]) and the Marion Plateau three sequences (Eberli et al., 2004); and the Torosa data (iii) differ from the Central Luconia platform FX system, which was progressively backstepping and drowning during this interval [11].

In total, the seismic stratigraphic characterization reveals that some global events are not clearly manifested in this area of the Northwest Shelf. Conversely, some marked events in this succession do not have parallels globally. Clearly, more local processes play important roles.

3.8. Regional and Local Influences on Seismic Geomorphology of Isolated Carbonate Platforms. Although several of the gross trends in stratigraphy and the ages of major bounding surfaces could be interpreted reasonably in the context of physical or chemical oceanographic processes of global scope (Figure 18), the high-resolution seismic data reveal another level of complexity. Several observations from comparing and contrasting patterns among platforms with these high-resolution data provide perspectives on the role of more local, dynamic processes and their influence on the architecture of isolated carbonate platforms.

A first observation is the marked heterogeneity evident within individual isolated platforms (Figures 9–16), even though they are relatively small (Figure 17). In contrast to platforms that are characterized by aggradational growth patterns and generally layer-cake internal geometries (e.g., Figure 19(b)) or aggradational then progradational geometries (e.g., [82, 83]; Sapardina et al. [84]), the Torosa data reveal much more complex architecture, reflected in variable patterns of birth and growth of platforms. For example, platforms may originate as clusters of small platforms several 100 m across that grow together and amalgamate into a larger platform (e.g., Figures 10–12), or as single broad, elongate features that build dominantly upward (e.g., Figures 15 and 16), before building outward. Likewise, with the exception of the smallest platforms (Figures 8(a) and 8(b)), almost no platforms appear to be simple, isotropic entities without internal seismic-stratal terminations (cf. Figure 19(b)). In fact, many platforms document several episodes of aggradation, progradation, and backstepping and can merge with adjacent platforms to form composite systems as well.

A second observation is the spatial and temporal variability in stratigraphic architecture among platforms of the same age (cf. [28, 85]). For example, consider UC-1 platforms. One platform (Figure 10) initiates as a generally circular to ovoid, low-relief platform. Above a flooding surface (S2), the platform backsteps to a W-NW/E-SE elongated platform, which then expands and grows to the N-NW. Another platform (Figure 11) initiated as a cluster of three low relief, slightly elongate buildups *ca* 1 km across. Above a flooding surface (R1), an aggradational phase built relief, and

subsequently, the platform expanded by progradation (compare Figures 11(c) and 11(e)). A minor flooding (surface R2) that placed downlapping slope deposits on top of platform-top strata was followed by more aggradation, with progradation of less than 200 m beyond the extent of the previous platform (Figure 11(f)). A final platform (Figure 12) initiates as two-low relief deposits that amalgamate into one elongate W-NW/E-SE oriented platform with *ca* 40 ms (68 m) relief (capped by H1). This platform is flanked by several prograding reflectors lower than the previous shelf margin, suggesting a relative fall in sea level (cf. [34]). This succession is reflooded, and the platform ultimately aggrades and progrades *ca* 750 m to the W-NW.

As illustrated by these divergent patterns, an interpretation of sea-level history derived solely on the basis of seismic-stratal geometries on one of two lines through one of these platforms, or even based on 3D data of solely one platform, could vary markedly, depending on the platform that was analyzed. Clearly, factors other than sea-level change (much less eustasy) influence these platforms, as discussed below. Nonetheless, relative changes in sea level of frequency higher than that reflected in the major bounding surfaces (e.g., surfaces bounding CPP-3 and CPP-4; [25]) did influence these systems, as evidenced by the terraces at positions lower than the previous shelf margin and the isolated platforms that initiated in paleo-lows of interplatform seaways (e.g., Figures 14 and 17).

A third observation regarding local processes is the propensity for these platforms be elongated from NW to SE and for the steeper margin to occur on the SE flanks and progradation more common on the NW margins. Such patterns commonly have been interpreted in the context of windward-leeward effects, as described for the middle and upper Miocene of the Bahamas (see above, [34]), older Miocene platforms from the Bonaparte Basin (north of the Browse Basin) [81], and Browse Basin buildups in the area just north of Torosa ([25], their Figure 5(c); [28]). This general paradigm, which predicts aggradation on high-energy windward margins, wind-driven cross-platform currents, and progradation off the low-energy leeward margin, has been used to interpret platforms throughout the geological record.

In this context, this pattern would suggest that the high-energy margin faced to the southeast in the Torosa area. These patterns are generally consistent with paleoclimate reconstructions, which suggest the area lay in the trade wind belt [86] with a weak to nonexistent monsoon in this area through the Miocene ([87]; cf. [11]). As such, the dominant easterly winds would favor eastern high-energy margins.

These patterns, and their interpretations, are opposite those illustrated elsewhere on Miocene platforms of the Northwest Shelf, however. For example, a study of older Miocene platforms from the Bonaparte Basin [81] documented fan-shaped depositional bodies, interpreted as fan aprons, on the northwestern flanks of platforms, a pattern that contrasted with more continuous margins with limited sediment shed to deeper water to the southeast. These patterns were interpreted to represent a windward flank to the northwest. Similarly, van Tuyl et al. [28] described numerous buildups in an area just north of Torosa with ubiquitous progradation towards the southeast. They interpreted the southwestward shedding to represent wind from the northwest, favoring progradation on a lower energy, leeward margin to the southeast. As it seems unlikely that winds shifted 180 degrees across less than 100 km, there likely are other interpretations.

Rather than reflecting energy variation solely related to the dominant wind, energy differences could reflect different exposures to open-ocean swell from the Indian Ocean. It could be that the barrier reef system west of Torosa survey area platforms protected platforms from this swell, which would in general terms come from the west. Belde et al. [25] describe the extensive CPP-3 barrier reef as extending from the south into the Torosa area, with individual platforms to the north, and then another "elongate reef front" farther north (cf. [29]). If protected, the higher-energy platform flank could be the landward, southeastern margin, and be most impacted by trade-wind-generated waves rather than by swell from the open Indian Ocean.

This scenario of more local control is consistent with the diversity of patterns documented around platforms of the Caribbean [88, 89] and Bahamas ([90–94]; Fauquembergue et al. [95]). In those examples, slope aprons and fans can occur on windward, waveward, and leeward margins; a universal, regionally consistent direction is absent.

Alternatively, or additionally, factors other than winds influence energy levels (cf. [7, 32, 74, 75]). The most likely influence would be currents, forces which could be influenced by wind-generated circulation, tides, or both. For example, Belde et al. [25] and van Tuyl et al. [28] suggested that currents played a progressively more influential role in shaping platforms through time and ultimately facilitated platform drownings. The results here are not inconsistent with such an interpretation. For example, the small UC-4 platform that lies in a concavity of the larger south UC-3 platform is less elongated than the platform in the passage between the north and south UC-3 platforms. The latter platform is markedly elongated, shaped by progradation of several km to the west (Figure 16). These differences may reflect focused, westward currents shaping the latter (Figure 16(d)), as the former was more protected until it was subsumed by progradation from the expanding south UC-3 platform (Figures 16(g) and 16(h)).

A final observation regarding these platforms is related to the range of sizes of the platforms. Although there is a clear trend towards larger platforms in the upper succession, there is a clear continuum, and no clear hierarchy; instead, the data reveal a power-law size-frequency distribution. These types of size-frequency distributions have been recognized in modern reef systems before (for example, [96, 97]), but not commonly in the rock record [98]. Rankey [96] tested various scenarios of growth dynamics for these types of distributions and suggested that they represent size-proportional and nonlinear growth of randomly aged and distributed features. In the context of the Torosa Miocene platforms, such an interpretation would suggest that platforms expand spatially at a rate that increases with size; their ages, or the duration from initiation to termination, would be random. The broadly smaller platforms in this area (Figure 17(i)) could reflect

more dynamic, and shorter-lived, systems here than in Central Luconia, where some Miocene platforms have persevered until the present, and on modern atolls, some of which originated in the Cretaceous.

Nonetheless, several other possibilities may explain some of the differences. First, tectonic setting clearly plays a role in influencing initiation and extent of platforms (e.g., [35, 99]). It is not evident why the tectonically active Central Luconia shelf would favor larger platforms than the passive margin Northwest Shelf, if tectonics were the fundamental control, however. Second, there may be a sampling bias. For example, Central Luconia data were mapped using lower-frequency data with the objective of identifying platforms that hold economically viable hydrocarbon reserves. As such, smaller or thinner platforms may occur, but not be mapped, because they are uneconomic. Similarly, some modern atolls are remnants of platforms that have survived tens of millions of years and may be biased towards larger systems. In contrast, the longest any CPP-3 or CPP-4 platform may have grown is much less than 10 Ma. A third reason for the differences may be distinct carbonate factories [100, 101], which can in turn influence production rates or geometries [62, 74]. As these specific Northwest Shelf platforms are undrilled and the flora and fauna are unknown, this possibility cannot be evaluated.

4. Conclusions

High-resolution seismic characterization of Middle to late Miocene isolated carbonate platforms of part of the Northwest Shelf, Australia, documents complex a history of birth, growth, and demise. Lower, CPP-3 (upper Langhian–early Tortonian) strata are up to 0.212 s (360 m) thick and include three seismic units (LC-0, LC-1, and LC-2) subdivided by surfaces mappable across the survey. LC-0 includes numerous small, small-relief platforms covered by prograding continuous reflectors, interpreted as shelf strata. LC-1 represents an eastward step of the shelf, with continued aggradation and progradation in some outboard isolated platforms. LC-2 includes expansion of the flat-topped, reef-rimmed platform across much of the area, passing eastward into slope and basinal deposits. The overlying CPP-4 (early Tortonian–Messinian) is up to 0.467 s (794 m) thick and includes six composite seismic sequences (UC-00, UC-0, UC-1, UC-2, UC-3, and UC-4). UC-00 and UC-0 include predominantly parallel, continuous to downlapping (basinal) reflectors, and is interpreted to represent a major flooding interval. In contrast, UC-1, UC-2, and UC-3 include numerous isolated platforms that are larger than those of the lower carbonate succession and include complex internal architecture. Mapping reveals isolated platforms of sizes from <400 m to >25 km across and <200 m synoptic relief and a power-law area-frequency distribution. UC-4 includes small platforms that nucleated in lows between preexisting platforms during a relative fall as well as expansion of UC-3 platforms following platform re-inundation.

These platforms initiated following the Middle Miocene Climatic Optimum, and the first-order patterns are consistent with global carbonate saturation state and eustatic trends. Interpretations of other Miocene platforms have emphasized the important role of these global processes on carbonate systems, and the first-order trends of initiation and platform phases appear to grossly correspond to eustatic and climatic trends. Nonetheless, the stratal variability and heterogeneity within and among platforms revealed by the high-resolution seismic data illustrate that regional tectonics and local oceanographic processes have a marked influence as well. The details of these sorts of dynamics likely are recorded in geomorphic and stratigraphic evolution of other platforms through geological history, but may be hidden in lower-frequency seismic data.

Data Availability

Seismic data are available from GeoScience Australia.

Conflicts of Interest

The authors declare that they have no conflicts of interest.

Acknowledgments

This research was funded by the Hubert and Kathleen Hall Professorship and by the sponsors of the Kansas Interdisciplinary Carbonates Consortium. Thanks are due to GeoScience Australia for making the seismic data available.

References

[1] R. N. Ginsburg, "Environmental relationships of grain size and constituent particles in some South Florida carbonate sediments," *AAPG Bulletin*, vol. 40, pp. 2384–2427, 1956.

[2] N. P. James, "The cool-water carbonate depositional realm," in *Cool-Water Carbonates*, N. P. James and J. A. D. Clarke, Eds., vol. 56, pp. 1–20, SEPM Society for Sedimentary Geology Special Publication, 1997.

[3] A. Lees, "Possible influence of salinity and temperature on modern shelf carbonate sedimentation," *Marine Geology*, vol. 19, no. 3, pp. 159–198, 1975.

[4] W. Schlager, "Accommodation and supply a dual control on stratigraphic sequences," *Sedimentary Geology*, vol. 86, no. 1-2, pp. 111–136, 1993.

[5] W. Schlager, "Carbonate Sedimentology and Sequence Stratigraphy," *SEPM Society for Sedimentary Geology Concepts in Sedimentology and Paleontology*, vol. 8, 2005.

[6] J. L. Wilson, *Carbonate Facies in Geologic History*, Springer-Verlag, New York, 1975.

[7] C. Betzler, G. P. Eberli, T. Lüdmann et al., "Refinement of Miocene sea level and monsoon events from the sedimentary archive of the Maldives (Indian Ocean)," *Progress in Earth and Planetary Science*, vol. 5, no. 1, 2018.

[8] C. Betzler, C. Hübscher, S. Lindhorst et al., "Monsoon-induced partial carbonate platform drowning (Maldives, Indian Ocean)," *Geology*, vol. 37, no. 10, pp. 867–870, 2009.

[9] B. P. Flower and J. P. Kennett, "The middle Miocene climatic transition: East Antarctic ice sheet development, deep ocean circulation and global carbon cycling," *Palaeogeography, Palaeoclimatology, Palaeoecology*, vol. 108, no. 3-4, pp. 537–555, 1994.

[10] J. Halfar and M. Mutti, "Global dominance of coralline red-algal facies: a response to Miocene oceanographic events," *Geology*, vol. 33, no. 6, pp. 481–484, 2005.

[11] M. Mathew, A. Makhankova, D. Menier, B. Sautter, C. Betzler, and B. Pierson, "The emergence of Miocene reefs in South China Sea and its resilient adaptability under varying eustatic, climatic and oceanographic conditions," *Scientific Reports*, vol. 10, no. 1, p. 7141, 2020.

[12] J. Zachos, M. Pagani, L. Sloan, E. Thomas, and K. Billups, "Trends, rhythms, and aberrations in global climate 65 Ma to present," *Science*, vol. 292, no. 5517, pp. 686–693, 2001.

[13] J. W. Snedden and C. Liu, "Recommendations for a uniform chronostratigraphic designation system for Phanerozoic depositional sequences," *American Association of Petroleum Geologists Bulletin*, vol. 95, no. 7, pp. 1095–1122, 2011.

[14] J. Sprintall, J. T. Potemra, S. L. Hautala, N. A. Bray, and W. W. Pandoe, "Temperature and salinity variability in the exit passages of the Indonesian Throughflow," *Deep-Sea Research*, vol. 50, no. 12-13, pp. 2183–2204, 2003.

[15] R. Wajsowicz, "Air-sea interaction over the Indian Ocean due to variations in the Indonesian Throughflow," *Climate Dynamics*, vol. 18, no. 5, pp. 437–453, 2002.

[16] P. J. Webster, V. O. Magana, T. N. Palmer et al., "Monsoons: processes, predictability, and the prospects for prediction," *Journal of Geophysical Research - Oceans*, vol. 103, no. C7, pp. 14451–14510, 1998.

[17] J. P. Kennett, G. Keller, and M. S. Srinivasan, "Miocene planktonic foraminiferal biogeography and paleoceanographic development of the Indo-Pacific region," in *The Miocene Ocean: Paleoceanography and Biogeography*, vol. 163 of Geological Society of America, pp. 197–236, 1985.

[18] W. Kuhnt, A. Holbourn, R. Hall, M. Zuvela, and R. Kaese, "Neogene history of the Indonesian Throughflow," in *Continent-Ocean Interactions Within East Asian Marginal Seas*, P. Clift, P. Wang, W. Kuhnt, and D. Hayes, Eds., vol. 149 of American Geophysical Union Geophysical Monographs Series, pp. 299–320, 2004.

[19] C. Betzler, G. P. Eberli, D. Kroon et al., "The abrupt onset of the modern South Asian Monsoon winds," *Scientific Reports*, vol. 6, no. 1, 2016.

[20] P. Baillie, C. M. C. A. Powell, Z.-X. Li, and A. M. Ryall, "Tectonic framework of Western Australia's Neoproterozoic to recent sedimentary basins," in *West Australian Basin Symposium*, pp. 45–62, Petroleum Exploration Society of Australia, Perth, 1994.

[21] M. Harrowfield and M. Keep, "Tectonic modification of the Australian North-West Shelf: episodic rejuvenation of long-lived basin divisions," *Basin Research*, vol. 17, no. 2, pp. 225–239, 2005.

[22] M. Keep, A. Bishop, and I. Longley, "Neogene wrench reactivation of the Barcoo Sub-basin, Northwest Australia: implications for Neogene tectonics of the northern Australian margin," *Petroleum Geoscience*, vol. 6, no. 3, pp. 211–220, 2000.

[23] B. Rosleff-Soerensen, L. Reuning, S. Back, and P. Kukla, "Seismic geomorphology and growth architecture of a Miocene barrier reef, Browse Basin, NW-Australia," *Marine and Petroleum Geology*, vol. 29, no. 1, pp. 233–254, 2012.

[24] B. Rosleff-Soerensen, L. Reuning, S. Back, and P. Kukla, "The response of a basin-scale Miocene barrier reef system to long-term, strong subsidence on a passive continental margin, Barcoo Sub-basin, Australian North West Shelf," *Basin Research*, vol. 28, no. 1, pp. 103–123, 2016.

[25] J. Belde, S. Back, J. Bourget, and L. Reuning, "Oligocene and Miocene carbonate platform development in the Browse Basin, Australian Northwest Shelf," *Journal of Sedimentary Research*, vol. 87, no. 8, pp. 795–816, 2017.

[26] V. Howarth and T. M. Alves, "Fluid flow through carbonate platforms as evidence for deep-seated reservoirs in Northwest Australia," *Marine Geology*, vol. 380, pp. 17–43, 2016.

[27] E. C. Rankey, "Seismic architecture and seismic geomorphology of heterozoan carbonates: Eocene-Oligocene, Browse Basin, Northwest Shelf, Australia," *Marine and Petroleum Geology*, vol. 82, pp. 424–443, 2017.

[28] J. Van Tuyl, T. M. Alves, and L. Cherns, "Geometric and depositional responses of carbonate build-ups to Miocene sea level and regional tectonics offshore Northwest Australia," *Marine and Petroleum Geology*, vol. 94, pp. 144–165, 2018.

[29] J. C. McCaffrey, M. W. Wallace, and S. J. Gallagher, "A Cenozoic Great Barrier Reef on Australia's North West Shelf," *Global and Planetary Change*, vol. 184, article 103048, 2020.

[30] G. R. Ramsayer, "Seismic stratigraphy, a fundamental exploration tool," in *Offshore Technology Conference*, vol. 11, pp. 101–109, Houston, Texas, 1979.

[31] S. L. Bachtel, H. W. Posamentier, and T. P. Gerber, "Seismic geomorphology and stratigraphic evolution of a Tertiary-aged isolated carbonate platform system, Browse Basin, North West Shelf of Australia, Part II," in *Seismic Imaging of Depositional and Geomorphic Systems: 30th Annual Gulf Coast Section, SEPM Society for Sedimentary Geology Foundation*, L. J. Wood, T. T. Simo, and N. C. Rosen, Eds., pp. 115–135, Bob F. Perkins Research Conference, Houston, TX, USA, 2011.

[32] S. L. Bachtel, R. D. Kissling, D. Martono, S. P. Rahardjanto, P. A. Dunn, and B. A. MacDonald, "Seismic stratigraphic evolution of the Miocene – Pliocene Segitiga Platform, East Natuna Sea, Indonesia: the origin, growth, and demise of an isolated carbonate platform," in *Seismic Imaging of Carbonate Reservoirs and Systems*, G. P. Eberli, J. L. Masaferro, and J. F. Sarg, Eds., vol. 81, pp. 309–328, American Association of Petroleum Geologists, Memoir, 2004.

[33] M. M. Saqab and J. Bourget, "Controls on the distribution and growth of isolated carbonate build-ups in the Timor Sea (NW Australia) during the Quaternary," *Marine and Petroleum Geology*, vol. 62, pp. 123–143, 2015.

[34] G. P. Eberli and R. N. Ginsburg, "Cenozoic progradation of NW Great Bahama Bank - a record of lateral platform growth and sea level fluctuations," in *Controls on Carbonate Platforms and Basin Development*, P. D. Crevello, J. L. Wilson, J. F. Sarg, and J. F. Read, Eds., vol. 44, pp. 339–355, Society of Economic Paleontologists and Mineralogists Special Publication, 1989.

[35] E. C. Rankey, "Deep-time perspectives on Miocene isolated carbonate platforms of Southeast Asia," in *Cenozoic Isolated Carbonate Platforms - Focus Southeast Asia*, E. C. Rankey and M. Poppelreiter, Eds., vol. 114, SEPM Society for Sedimentary Geology Special Publication, 2020.

[36] E. G. Purdy and E. L. Winterer, "Origin of atoll lagoons," *Geological Society of America Bulletin*, vol. 113, no. 7, pp. 837–854, 2001.

[37] M. E. Wilson, "Global and regional influences on equatorial shallow-marine carbonates during the Cenozoic,"

Palaeogeography, Palaeoclimatology, Palaeoecology, vol. 265, no. 3-4, pp. 262–274, 2008.

[38] S. S. Berhad, S. Lutong, and M. Epting, "Sedimentology of Miocene carbonate buildups, central Luconia, offshore Sarawak," *Bulletin of the Geological Society of Malaysia*, vol. 12, pp. 17–30, 1980.

[39] E. Koša, G. M. D. Warrlich, and G. Loftus, "Wings, mushrooms, and Christmas trees: the carbonate seismic geomorphology of Central Luconia, Miocene–present, offshore Sarawak, northwest Borneo," *AAPG Bulletin*, vol. 99, pp. 2043–2075, 2015.

[40] V. C. Vahrenkamp, "Miocene carbonates of the Luconia province, offshore Sarawak: implications for regional geology and reservoir properties from strontium-isotope stratigraphy," *Geological Society of Malaysia Bulletin*, vol. 42, pp. 1–13, 1998.

[41] E. Koša, "Sea-level changes, shoreline journeys, and the seismic stratigraphy of Central Luconia, Miocene–Present, offshore Sarawak, NW Borneo," *Marine and Petroleum Geology*, vol. 59, pp. 35–55, 2015.

[42] K.-K. Ting, B. J. Pierson, O. Al-Jaaidi, and P. Hague, "Effects of syn-depositional tectonics on platform geometry and reservoir characers in Miocene carbonate platforms of Central Luconia, Sarawak," in *International Petroleum Technology Conference*, Bangkok, Thailand, 2011.

[43] M. Y. Ali, *An integrated analysis of the depositional control, sedimentology, and diagenesis of Cenozoic carbonates from the Sarawak Basin, East Malaysia*, Imperial College, London, 2013.

[44] E. C. Rankey, M. Schlaich, S. Mokhtar, G. Ghon, H. Ali, and M. Poppelreiter, "Seismic architecture of a Miocene isolated carbonate platform and associated off-platform strata (Central Luconia Province, Offshore Malaysia)," *Marine and Petroleum Geology*, vol. 102, pp. 477–495, 2019.

[45] S. S. Berhad, S. Lutong, and K. F. Ho, "Stratigraphic framework for oil exploration in Sarawak," *Geological Society of Malaysia Bulletin*, vol. 10, pp. 1–13, 1978.

[46] J. L. Masaferro, R. Bourne, and J. C. Jauffred, "Three-dimensional seismic volume visualization of carbonate reservoirs and structures," in *Seismic Imaging of Carbonate Reservoirs and Systems*, G. P. Eberli, J. L. Masaferro, and J. F. Sarg, Eds., vol. 81, pp. 11–41, American Association of Petroleum Geologists Memoir, 2004.

[47] V. Zampetti, W. Schlager, J.-H. van Konijnenburg, and A. J. Everts, "Architecture and growth history of a Miocene carbonate platform from 3D seismic reflection data; Luconia Province, offshore Sarawak, Malaysia," *Marine and Petroleum Geology*, vol. 21, no. 5, pp. 517–534, 2004.

[48] O. Aubert and A. W. Droxler, "General Cenozoic evolution of the Maldives carbonate system (equatorial Indian Ocean)," *Bulletin Centers Research Exploration and Production Elf-Aquitaine*, vol. 16, pp. 113–136, 1992.

[49] A. V. Belopolsky and A. W. Droxler, "Seismic expressions of prograding carbonate bank margins: middle Miocene progradation in the Maldives, Indian Ocean," in *Seismic Imaging of Carbonate Reservoirs and Systems*, G. P. Eberli, J. L. Masaferro, and J. F. Sarg, Eds., vol. 81, pp. 267–290, American Association of Petroleum Geologists, Memoir, 2004.

[50] C. Betzler, J. Fürstenau, T. Lüdmann et al., "Sea-level and ocean-current control on carbonate platform growth, Maldives, Indian Ocean," *Basin Research*, vol. 25, no. 2, pp. 172–196, 2013.

[51] J. Reolid, C. Betzler, and T. Lüdmann, "Facies and sedimentology of a carbonate delta drift (Miocene, Maldives)," *Sedimentology*, vol. 66, no. 4, pp. 1243–1265, 2019.

[52] J. Reolid, C. Betzler, J. C. Braga, T. Lüdmann, A. Ling, and G. P. Eberli, "Facies and geometry of drowning steps in a Miocene carbonate platform (Maldives)," *Palaeogeography, Palaeoclimatology, Palaeoecology*, vol. 538, p. 109455, 2020.

[53] J. W. Ladd and R. E. Sheridan, "Seismic stratigraphy of the Bahamas," *AAPG Bulletin*, vol. 71, pp. 719–736, 1987.

[54] G. P. Eberli and R. N. Ginsburg, "Segmentation and coalescence of Cenozoic carbonate platforms, northwestern Great Bahama Bank," *Geology*, vol. 15, pp. 75–79, 1987.

[55] G. P. Eberli, F. S. Anselmetti, D. Kroon, T. Sato, and J. D. Wright, "The chronostratigraphic significance of seismic reflections along the Bahamas transect," *Marine Geology*, vol. 185, no. 1-2, pp. 1–17, 2002.

[56] G. P. Eberli, P. K. Swart, D. F. McNeill et al., "A synopsis of the Bahamas Drilling Project: results from two deep core borings drilled on the Great Bahama Bank," in *Proceedings of the Ocean Drilling Program, Initial Reports*, G. P. Eberli, P. K. Swart, M. Malone, and J. F. Sarg, Eds., vol. 166, pp. 23–41, 1997.

[57] C. Manfrino and R. N. Ginsburg, "Pliocene to pleistocene depositional history of the upper platform margin," in *Subsurface Geology of a Prograding Carbonate Platform Margin, Great Bahama Bank*, R. N. Ginsburg, Ed., vol. 70, pp. 17–39, SEPM Society for Sedimentary Geology Special Publication, 2001.

[58] F. S. Anselmetti, G. P. Eberli, and Z.-D. Ding, "From the Great Bahama Bank into the Straits of Florida: A margin architecture controlled by sea-level fluctuations and ocean currents," *Geological Society of America Bulletin*, vol. 112, no. 6, pp. 829–844, 2000.

[59] B. U. Haq, J. Hardenbol, and P. R. Vail, "Chronology of fluctuating sea levels since the Triassic," *Science*, vol. 235, no. 4793, pp. 1156–1167, 1987.

[60] G. P. Eberli, "The record of Neogene sea-level changes in the prograding carbonates along the Bahamas Transect—Leg 166 synthesis," in *Proceedings of the Ocean Drilling Program, Scientific Results*, P. K. Swart, G. P. Eberli, M. J. Malone, and J. F. Sarg, Eds., vol. 166, pp. 167–177, 2000.

[61] P. J. Davies, P. A. Symonds, D. A. Feary, and C. J. Pigram, "The evolution of the carbonate platforms of Northeast Australia," in *Controls on Carbonate Platforms and Basin Development*, P. D. Crevello, J. L. Wilson, J. F. Sarg, and J. F. Read, Eds., vol. 44, pp. 233–258, SEPM Society for Sedimentary Geology Special Publication, 1989.

[62] C. Betzler, D. Kroon, S. Gartner, and W. Wei, "Eocene to Miocene chronostratigraphy of the Queensland Plateau: control of climate and sea level on platform evolution," in *Proceedings of the Ocean Drilling Program, Scientific Results*, J. A. McKenzie, P. J. Davies, A. Palmer-Julson, and the Shipboard Scientific Party, Eds., vol. 133, pp. 281–289, 1993.

[63] J. A. McKenzie and P. J. Davies, "Cenozoic evolution of carbonate platforms on the northeastern Australian margin: synthesis of Leg 133 drilling results," in *Proceedings of the Ocean Drilling Program, Scientific Results*, J. A. McKenzie, P. J. Davies, A. Palmer-Julson, and the Shipboard Scientific Party, Eds., vol. 133, pp. 763–770, 1993.

[64] C. Betzler, T. C. Brachert, and D. Kroon, "Role of climate in partial drowning of the Queensland Plateau carbonate

platform (northeastern Australia)," *Marine Geology*, vol. 123, no. 1-2, pp. 11–32, 1995.

[65] A. R. Edwards, "Southwest Pacific Cenozoic paleogeography and an integrated Neogene paleocirculation model," in *Initial Reports of the Deep Sea Drilling Project, Initial Reports*, J. E. Andrews, G. Packham, and J. Herring, Eds., vol. 30, pp. 667–684, 1975.

[66] A. R. Isern, J. A. McKenzie, and D. W. Müller, "Paleoceanographic changes and reef growth off the northeastern Australian margin: stable isotopic data from ODP leg 133 sites 811 and 817 and DSDP leg 21 site 209," in *Proceedings of the Ocean Drilling Program, Scientific Results*, J. A. McKenzie, P. J. Davies, A. Palmer-Julson, and the Shipboard Scientific Party, Eds., vol. 133, pp. 263–280, 1993.

[67] M. Lyle, K. A. Dadey, and J. W. Farrell, "The late miocene (11-8 Ma) Eastern Pacific carbonate crash: evidence for reorganization of deep-water circulation by the closure of the panama gateway," in *Proceedings of Ocean Drilling Program, Scientific Results*, N. G. Pisias, L. A. Mayer, T. R. Janecek, A. Palmer-Julson, and T. H. Andel, Eds., vol. 138, pp. 821–838, 1995.

[68] J. Lübbers, W. Kuhnt, A. E. Holbourn et al., "The middle to late Miocene "Carbonate Crash" in the equatorial Indian Ocean," *Paleoceanography and Paleoclimatology*, vol. 34, pp. 813–832, 2019.

[69] J. M. Roth, A. W. Droxler, and K. Kameo, "The Caribbean carbonate crash at the middle to late Miocene transition: linkage to the establishment of the modern global ocean conveyor," in *Proceedings of the Ocean Drilling Program, Scientific Results*, vol. 165, pp. 249–273, 2000.

[70] A. R. Isern, F. S. Anselmetti, and P. Blum, "Constraining Miocene sea-level change from carbonate platform evolution, Marion Plateau, Northeast Australia, Sites 1192-1199," *Proceedings of the Ocean Drilling Program, Initial Reports*, vol. 194, pp. 1–88, 2002.

[71] C. M. John, G. D. Karner, and M. Mutti, "$\delta^{18}O$ and Marion Plateau backstripping: combining two approaches to constrain late middle Miocene eustatic amplitude," *Geology*, vol. 32, no. 9, pp. 829–832, 2004.

[72] S. N. Ehrenberg, J. M. McArthur, and M. F. Thirlwall, "Growth, demise, and dolomitization of Miocene carbonate platforms on the Marion Plateau, offshore NE Australia," *Journal of Sedimentary Research*, vol. 76, no. 1, pp. 91–116, 2006.

[73] P. Kindler, C. Ruchonnet, and T. White, "The Southern Marion Platform (Marion Plateau, NE Australia) during the early Pliocene: a lowstand-producing, temperate-water carbonate factory," *Geological Society, London, Special Publications*, vol. 255, no. 1, pp. 269–282, 2006.

[74] G. P. Eberli, F. S. Anselmetti, A. R. Isern, and H. Delius, "Timing of changes in sea-level and currents along Miocene platforms on the Marion Plateau, Australia," in *Cenozoic Carbonate Systems of Australasia*, W. A. Morgan, A. D. George, P. M. Harris, J. A. Kupecz, and J. F. Sarg, Eds., vol. 95, pp. 221–243, SEPM Society for Sedimentary Geology Special Publication, 2010.

[75] A. Isern, F. S. Anselmetti, and P. Blum, "A Neogene carbonate platform, slope and shelf edifice shaped by sea level and ocean currents, Marion Plateau (Northeast Australia)," in *Seismic Imaging of Carbonate Reservoirs and Systems*, G. P. Eberli, J. L. Masaferro, and J. F. Sarg, Eds., vol. 81, pp. 291–307, American Association of Petroleum Geologists Memoir, 2004.

[76] C. Betzler, D. Kroon, and J. J. Reijmer, "Synchroneity of major late Neogene sea level fluctuations and paleoceanographically controlled changes as recorded by two carbonate platforms," *Paleoceanography and Paleoclimatology*, vol. 15, pp. 722–730, 2000.

[77] T. C. Brachert, C. Betzler, P. J. Davies, and D. A. Feary, "Climatic change: Control of carbonate platform development (Eocene-Miocene, Leg 133, Northeastern Australia," in *Proceedings of the Ocean Drilling Program, Scientific Results*, J. A. McKenzie, P. J. Davies, A. Palmer-Julson, and the Shipboard Scientific Party, Eds., vol. 133, pp. 291–300, 1993.

[78] J. W. Snedden and C. Liu, "A compilation of Phanerozoic Sea-level change, coastal onlaps and recommended sequence designations: Search and Discovery Article #40594," 2010.

[79] B. P. Boudreau, J. J. Middelburg, A. Sluijs, and R. van der Ploeg, "Secular variations in the carbonate chemistry of the oceans over the Cenozoic," *Earth and Planetary Science Letters*, vol. 512, pp. 194–206, 2019.

[80] K. Czarnota, M. J. Hoggard, N. White, and J. Winterbourne, "Spatial and temporal patterns of Cenozoic dynamic topography around Australia," *Geochemistry, Geophysics, Geosystems*, vol. 14, no. 3, pp. 634–658, 2013.

[81] M. M. Saqab and J. Bourget, "Seismic geomorphology and evolution of early–mid Miocene isolated carbonate buildups in the Timor Sea, North West Shelf of Australia," *Marine Geology*, vol. 379, pp. 224–245, 2016.

[82] D. J. Lehrmann, Wei Jiayong, and P. Enos, "Controls on facies architecture of a large Triassic carbonate platform: the Great Bank of Guizhou, Nanpanjiang basin, South China," *Journal of Sedimentary Research*, vol. 68, no. 2, pp. 311–326, 1998.

[83] A. H. Saller and S. Vijaya, "Depositional and diagenetic history of the Kerendan carbonate platform, Oligocene, Central Kalimantan, Indonesia," *Journal of Petroleum Geology*, vol. 25, no. 2, pp. 123–149, 2002.

[84] D. Sapardina, R. Sekti, F. Musgrove, and N. Stephens, "Tight rinds in SE Asia Oligo-Miocene isolated carbonate platforms," in *Proceedings, Indonesian Petroleum Association, Paper IPA13-G-195*, Jakarta, Indonesia, 2013.

[85] K.-K. Ting, Y. T. Eng, C. Edwin, L. E. Lin, A. N. Azudin, and N. A. Ishak, "Assessing controls on isolated carbonate platform development in Central Luconia, NW Borneo, from a regional 3D seismic facies and geomorphology investigation," in *Seismic Characterisation of Carbonate Platforms and Reservoirs*, J. Hendry and V. Zampetti, Eds., Geological Society of London Special Publication, 2020.

[86] J. Groeneveld, J. Henderiks, W. Renema et al., "Australian shelf sediments reveal shifts in Miocene Southern Hemisphere westerlies," *Science Advances*, vol. 3, no. 5, article e1602567, 2017.

[87] N. Herold, M. Huber, R. D. Müeller, and M. Seton, "Modeling the Miocene climatic optimum: ocean circulation," *Paleoceanography*, vol. 27, article PA1209, 2011.

[88] N. Andresen, J. J. G. Reijmer, and A. W. Droxler, "Timing and distribution of calciturbidites around a deeply submerged carbonate platform in a seismically active setting (Pedro Bank, Northern Nicaragua Rise, Caribbean Sea)," *International Journal of Earth Sciences*, vol. 92, no. 4, pp. 573–592, 2003.

[89] B. D. Bornhold and O. H. Pilkey, "Bioclastic turbidite sedimentation in Columbus Basin, Bahamas," *Geological Society of America Bulletin*, vol. 82, no. 5, pp. 1341–1354, 1971.

[90] L. Chabaud, E. Ducassou, E. Tournadour et al., "Sedimentary processes determining the modern carbonate periplatform drift of Little Bahama Bank," *Marine Geology*, vol. 378, pp. 213–229, 2016.

[91] P. D. Crevello and W. Schlager, "Carbonate debris sheets and turbidites, Exuma Sound, Bahamas," *SEPM Journal of Sedimentary Research*, vol. 50, pp. 1121–1148, 1980.

[92] T. Mulder, H. Gillet, V. Hanquiez et al., "Carbonate slope morphology revealing a giant submarine canyon (Little Bahama Bank, Bahamas)," *Geology*, vol. 46, no. 1, pp. 31–34, 2017.

[93] W. Schlager and A. Chermak, "Sediment facies of platform-basin transition, Tongue of the Ocean, Bahamas," in *Geology of Continental Slopes*, L. J. Doyle and O. H. Pilkey, Eds., vol. 27, pp. 193–208, SEPM Society for Sedimentary Geology Special Publication, 1979.

[94] E. Tournadour, T. Mulder, J. Borgomano, V. Hanquiez, E. Ducassou, and H. Gillet, "Origin and architecture of a mass transport complex on the northwest slope of Little Bahama Bank (Bahamas): relations between off-bank transport, bottom current sedimentation and submarine landslides," *Sedimentary Geology*, vol. 317, pp. 9–26, 2015.

[95] K. Fauquembergue, E. Ducassou, T. Mulder et al., "Genesis and growth of a carbonate Holocene wedge on the northern Little Bahama Bank," *Marine and Petroleum Geology*, vol. 96, pp. 602–614, 2018.

[96] E. C. Rankey, "On facies belts and facies mosaics: Holocene isolated platforms, South China Sea," *Sedimentology*, vol. 63, no. 7, pp. 2190–2216, 2016.

[97] W. Schlager and S. J. Purkis, "Bucket structure in carbonate accumulations of the Maldive, Chagos, and Laccadive archipelagos," *International Journal of Earth Science*, vol. 102, no. 8, pp. 2225–2238, 2013.

[98] S. J. Purkis, G. Casini, D. Hunt, and A. Colpaert, "Morphometric patterns in modern carbonate platforms can be applied to the ancient rock record: similarities between modern Alacranes Reef and upper Palaeozoic platforms of the Barents Sea," *Sedimentary Geology*, vol. 321, pp. 49–69, 2015.

[99] D. Bosence, "A genetic classification of carbonate platforms based on their basinal and tectonic settings in the Cenozoic," *Sedimentary Geology*, vol. 175, no. 1-4, pp. 49–72, 2005.

[100] L. Pomar, "Types of carbonate platforms: a genetic approach," *Basin Research*, vol. 13, no. 3, pp. 313–334, 2001.

[101] W. Schlager, "Benthic carbonate factories of the Phanerozoic," *International Journal of Earth Sciences*, vol. 92, no. 4, pp. 445–464, 2003.